# Initiation of translation on nedicistrovirus and related intergenic region IRESs by their factor-independent binding to the P site of 80S ribosomes

ANNA MIŚCICKA,[1] KRISTEN LU,[1] IRINA S. ABAEVA, TATYANA V. PESTOVA, and CHRISTOPHER U.T. HELLEN

Department of Cell Biology, SUNY Downstate Health Sciences University, Brooklyn, New York 11203, USA

## ABSTRACT

**Initiation of translation on many viral mRNAs occurs by noncanonical mechanisms that involve 5′ end-independent binding of ribosomes to an internal ribosome entry site (IRES). The ∼190-nt-long intergenic region (IGR) IRES of dicistroviruses such as cricket paralysis virus (CrPV) initiates translation without Met-tRNA$_i^{Met}$ or initiation factors. Advances in metagenomics have revealed numerous dicistrovirus-like genomes with shorter, structurally distinct IGRs, such as nedicistrovirus (NediV) and Antarctic picorna-like virus 1 (APLV1). Like canonical IGR IRESs, the ∼165-nt-long NediV-like IGRs comprise three domains, but they lack key canonical motifs, including L1.1a/L1.1b loops (which bind to the L1 stalk of the ribosomal 60S subunit) and the apex of stem–loop V (SLV) (which binds to the head of the 40S subunit). Domain 2 consists of a compact, highly conserved pseudoknot (PKIII) that contains a UACUA loop motif and a protruding CrPV-like stem–loop SLIV. In vitro reconstitution experiments showed that NediV-like IRESs initiate translation from a non-AUG codon and form elongation-competent 80S ribosomal complexes in the absence of initiation factors and Met-tRNA$_i^{Met}$. Unlike canonical IGR IRESs, NediV-like IRESs bind directly to the peptidyl (P) site of ribosomes leaving the aminoacyl (A) site accessible for decoding. The related structures of NediV-like IRESs and their common mechanism of action indicate that they exemplify a distinct class of IGR IRES.**

**Keywords: dicistrovirus; nedicistrovirus; Antarctic picorna-like virus 1; IRES; ribosome; translation initiation**

## INTRODUCTION

The canonical eukaryotic translation initiation mechanism involves more than 10 eukaryotic initiation factors (eIFs) (Jackson et al. 2010). Binding of eIF4F to the capped 5′-end of mRNA promotes recruitment of the ribosomal 43S preinitiation complex, which scans to the AUG initiation codon to form a 48S complex. Subsequent subunit joining and factor displacement yield an elongation-competent ribosome with initiator tRNA and the AUG codon base-paired in the P site.

Viruses co-opt the host translation machinery and often use alternative cap-independent mechanisms to initiate translation, for example on internal ribosome entry sites (IRESs), that require only a subset of eIFs. Such mechanisms enable viral mRNAs to evade innate immune responses that inactivate specific eIFs, and to gain preferential access to the translation apparatus following inactivation of eIFs that are required for canonical but not for IRES-mediated initiation. IRESs are structured *cis*-acting elements in mRNAs that interact with the translation apparatus to mediate 5′ end-independent recruitment of initiation complexes. Several classes of IRES have been identified, each with a characteristic structure and conserved sequence motifs, but there is no consensus regarding their nomenclature (Kieft 2008; Jackson et al. 2010; Mailliot and Martin 2018; Martinez-Salas et al. 2018). We therefore proposed that the different classes be designated type 1 (e.g., poliovirus), type 2 (encephalomyocarditis virus), type 3 (hepatitis A virus [HAV]), type 4 (hepatitis C virus [HCV]), type 5 (e.g., kobuvirus), and type 6 (dicistrovirus IGRs) (Arhab et al. 2020, 2022).

The two major subclasses of type 6 IRES are type 6a (epitomized by CrPV and *Plautia stali* intestine virus) (Sasaki and Nakashima 1999, 2000; Wilson et al. 2000a) and type 6b (e.g., Taura syndrome virus [TSV] and Israeli acute paralysis virus) (Fig. 1; Hatakeyama et al. 2004; Ren et al. 2012). They have a bipartite structure, in which the nested pseudoknots

[1]These authors contributed equally to this work.

**Corresponding author: christopher.hellen@downstate.edu**

Article is online at http://www.rnajournal.org/cgi/doi/10.1261/rna.079599.123.

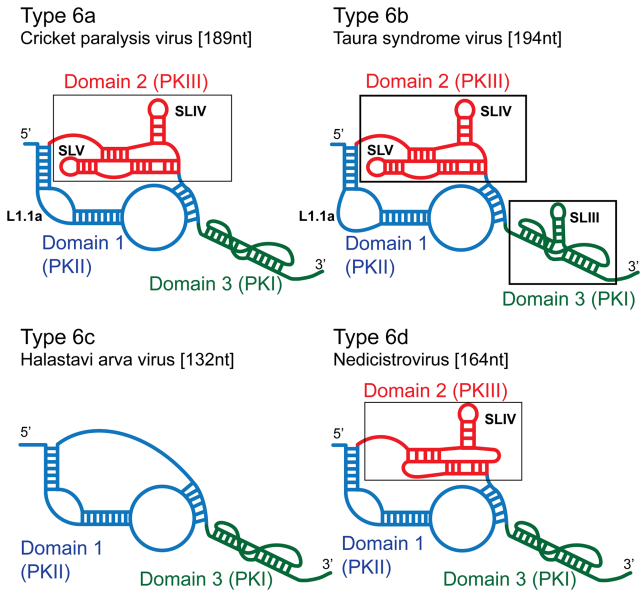


**FIGURE 1.** Schematic models of different types of IGR IRES. Models of (*A*) a type 6a IRES (e.g., cricket paralysis virus), (*B*) a type 6b IRES (e.g., Taura syndrome virus), (*C*) a type 6c IRES (e.g., Halastavi árva virus), and (*D*) a type 6d IRES (e.g., nedicistrovirus), labeled to indicate domain 1 (PKII) colored blue, domain 2 (PKIII) colored red and domain 3 (PKI) colored green, stem–loops SLIII, SLIV, and SLV, and the L1.1a loop.

PKII (domain 1) and particularly PKIII (domain 2) are primarily responsible for the affinity of binding of the IRES to the ribosome (Nishiyama et al. 2003; Costantino and Kieft 2005). The L1.1 loop in PKII binds to the L1 stalk of the 60S subunit, and stem–loop (SL) IV and SLV in PKIII bind to the head of the 40S subunit (Schüler et al. 2006; Fernández et al. 2014). PKI (domain 3) establishes the translational reading frame by mimicking the anticodon stem–loop (ASL) of tRNA base-paired to a cognate mRNA codon (Costantino et al. 2008). Type 6b IRESs have a larger L1.1a loop than type 6a IRESs, and an additional hairpin (SLIII) in PKI. Some sequence motifs in these IRESs are conserved, but the function of many structural elements is sequence-independent, so that loss of function caused by destabilizing substitutions is restored by compensatory second-site substitutions (Sasaki and Nakashima 2000; Jan and Sarnow 2002). The third subclass, type 6c, is epitomized by Halastavi árva virus (HalV) (Fig. 1). It contains PKI and PKII pseudoknots and a single-stranded linker in place of PKIII (Abaeva et al. 2020).

IGR IRESs promote initiation without the involvement of an AUG codon, initiator tRNA or eIFs either by binding to a 40S subunit followed by recruitment of a 60S subunit or by binding directly to a ribosome (Wilson et al. 2000a; Jan et al. 2003; Pestova and Hellen 2003; Pestova et al. 2004). Type 6a and 6b IRESs bind in the intersubunit space, inserting PKI into the decoding center of the A site (Zhu et al. 2011; Fernández et al. 2014; Koh et al. 2014). eEF2 promotes translocation of PKI to the P site, placing the first codon of the open reading frame in the A site where it can be decoded by cognate eEF1A-GTP/aa-tRNA (Fernández et al. 2014). A second round of eEF2-mediated translocation moves the aa-tRNA to the P site and the IRES to the exit (E) site, yielding an elongation-competent ribosome (Pisareva et al. 2018). The divergent type 6c HalV IRES binds stably to ribosomes but not to 40S subunits, and in contrast to 6a and 6b IRESs, binds directly to the P site, so that the first codon can be decoded without a prior translocation step (Abaeva et al. 2020).

Advances in metagenomic analysis have greatly increased the number of known dicistro-like viral genomes (e.g., Shi et al. 2016; Waldron et al. 2018; Wolf et al. 2020; Chen et al. 2022; Edgar et al. 2022; Yang et al. 2022; Zell et al. 2022). Many of them contain IGRs that are shorter than type 6a and 6b IRESs and either lack or contain divergent versions of conserved sequence motifs. These differences suggest that if these IGRs function as IRESs, they may utilize novel initiation mechanisms. Here, we characterized the structures and mechanism of action of the ~165-nt-long nedicistrovirus (NediV) and Antarctic picorna-like virus 1 (APLV1) IGRs (Ng et al. 2012; López-Bueno et al. 2015).

## RESULTS

### Structural models of NediV-like IGR IRESs

NediV and APLV1 IGRs share ~60% sequence identity and thus likely have similar structures. Related IGRs (36%–92% pairwise sequence identity) occur in Beihai picorna-like virus 78, Changjiang picorna-like virus 9 and Sanxia picorna-like virus 12 (Shi et al. 2016), *Gingko biloba* dicistrovirus strain pt112-dic-11 (Yang et al. 2022), Picornavirales sp. isolates s64-k141_2464283 and R35-k141_316374 (Chen et al. 2022), and a Transcriptome Shotgun Assembly (TSA) sequence from *Pallasea cancelloides* (Fig. 2A; Naumenko et al. 2017). These IGRs are located between open reading frames ORF1 and ORF2 that encode nonstructural and structural protein precursors, respectively, that are homologous to polyproteins encoded by members of *Dicistroviridae*. These sequences were derived from environmental samples and from members of the phyla *Arthropoda* and *Mollusca*.

The putative IRESs are similar in size (161–168 nt from the 5′ border up to and including the putative GCU or ACU initiation codons). They are ~25 nt shorter than type 6a IRESs but have a similar predicted three-domain structure (Fig. 2B,C). Domain 1 comprises a pseudoknot (PKII), helix P1.1 (which overlaps or is adjacent to the ORF1 stop codon), helices P1.2 and P1.3, and internal loops L1.1a/L1.1b and L1.2a/L1.2b. Conserved UAUACG and G(U/A)CAGG motifs in the L1.1a/L1.1b loops differ from the corresponding U[G/A]A[U/C]C and UGCUA

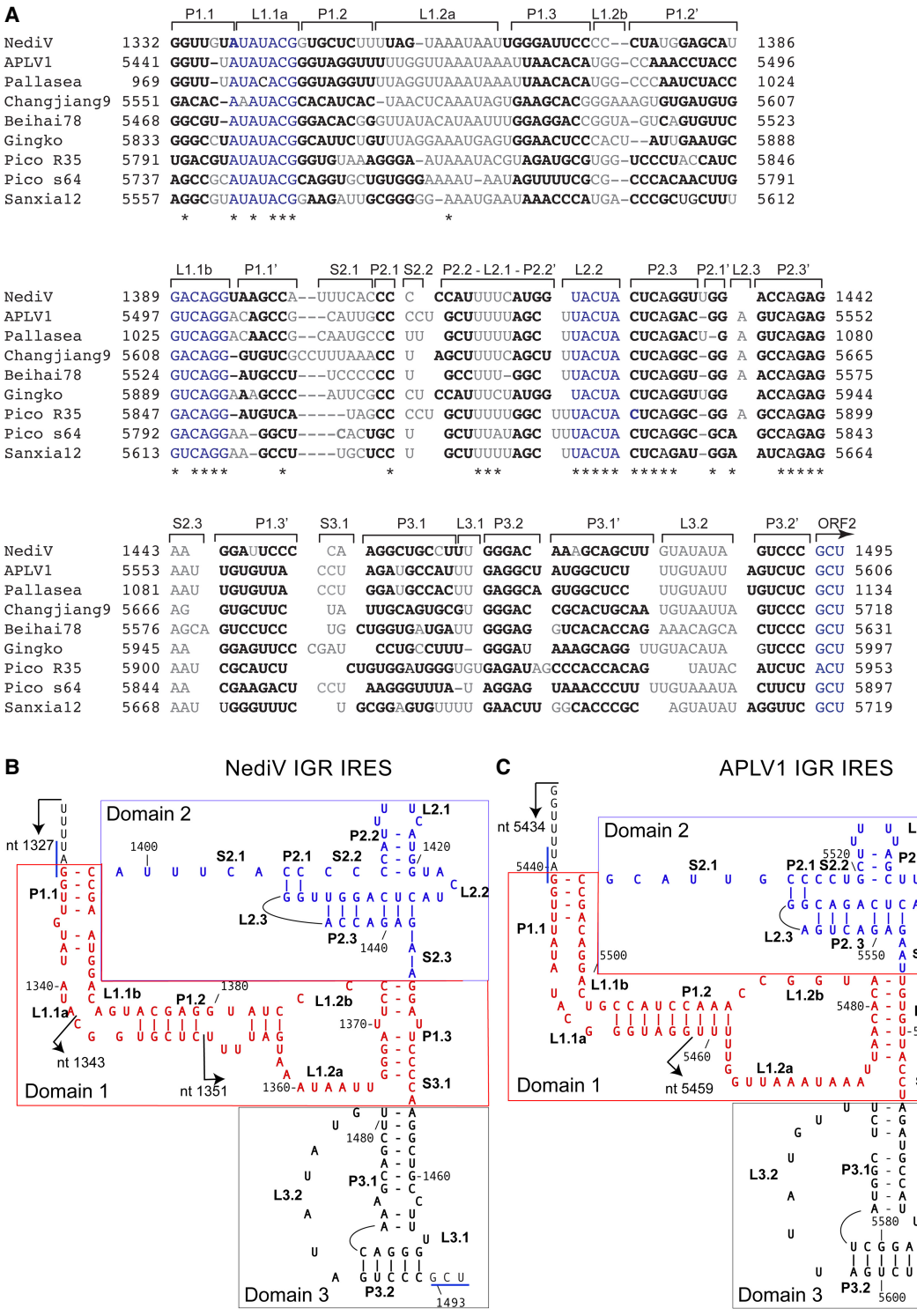


**FIGURE 2.** Sequence alignments and structural models of NediV and APLV1 IGR IRESs. (*A*) Aligned sequences from nedicistrovirus (NediV), Antarctic picorna-like virus 1 (APLV1), a viral TSA fragment from *Pallasea cancelloides* (Pallasea), Changjiang picorna-like virus 9 (Changjiang9), Beihai picorna-like virus 78 (Beihai78), *Gingko biloba* dicistrovirus (Gingko), Picornavirales sp. isolates R35-k141_316374 (Pico R35) and s64-k141_2464283 (Pico s64), and Sanxia picorna-like virus 12 (Sanxia12), annotated to show nucleotide numbers, structural elements (as in panels *B*, *C*), the ORF2 initiation codon, conserved sequence motifs (blue), base-paired nucleotides (bold), unpaired residues (light gray or light blue), and conserved nucleotides (indicated by asterisks). (*B*,*C*) Models of (*B*) NediV and (*C*) APLV1 IRESs. Nucleotides are numbered at 20-nt intervals. Domains 1 (PKII), 2 (PKIII), and 3 (PKI) are colored red, blue, and black, respectively. The 5′ borders of truncated IGR mRNAs used to define the IRES 5′ border (see Fig. 4A,B) are indicated by arrows. The NediV codon $GCU_{1493–5}$ and the APLV1 codon $GCU_{5604–6}$ that predominantly occupy the A site on initial binding of ribosomes, and the NediV $UAG_{1330–2}$ and APLV1 $UAG_{5439–41}$ ORF1 stop codons are indicated by blue lines.

motifs in type 6a, 6b, and 6c IRESs (Nakashima and Uchiumi 2009; Abaeva et al. 2020). Domain 3 consists of a pseudoknot (PKI) followed by the first codon of ORF2. Domain 2 differs significantly from the corresponding region in CrPV-like IRESs: like them, it contains a pseudoknot with a protruding SLIV-like hairpin with a pyrimidine-rich loop (L2.1), but it lacks SLV, and it contains a conserved UACUA loop motif (L2.2) adjacent to the SLIV-like hairpin that is unique to NediV-like IGRs. They therefore constitute a distinct subset of IRES, designated here as type 6d (Fig. 1).

## Factor-independent attachment of ribosomes to NediV-like IGR IRESs

APLV1 and NediV are representative of these putative IRESs. We used in vitro reconstitution to verify that they promote internal ribosomal entry and to characterize their mechanism of action. Ribosomal complexes were assembled from purified ribosomal subunits, factors and aminoacyl-tRNAs (mammalian, unless otherwise stated) on mRNAs that consisted of a stable 5′-terminal hairpin to block 5′ end-dependent initiation (Babendure et al. 2006) followed by NediV nt 1161–1606 or APLV1 nt 5337–5772. The positions of ribosomal complexes on these mRNAs were mapped by toeprinting, in which extension by reverse transcriptase of a primer annealed to mRNA is arrested at the leading edge of stably bound 40S subunits, 48S complexes and 80S ribosomes, yielding toeprints +15–17 nt from the first nucleotide of the P site codon.

In contrast to the CrPV IGR IRES but like that of HalV (Abaeva et al. 2020), NediV and APLV1 IGRs did not bind to 40S subunits to yield toeprints that are indicative of stable binding of the IRES in the mRNA-binding cleft (Fig. 3A, lanes 2,5,8; Fig. 3B, lanes 2,5,8). However, they bound to 80S ribosomes independently of initiation factors like all IGR IRESs (Fig. 3A, lanes 3,6,9; Fig. 3B, lanes 3,6,9). Ribosomes bound to the NediV IGR yielded strong toeprints +15–17 nt from $CCC_{1490–2}$, the triplet in PKI immediately upstream of the predicted $GCU_{1493–5}$ start codon: these toeprints correspond to binding of $CCC_{1490–2}$ in the P site (Fig. 3A, lane 3). Ribosomes bound to the APLV1 IGR yielded toeprints +16–17 nt relative to $CUC_{5601–3}$ (Fig. 3B, lane 3). Their appearance indicates that NediV and APLV1 IGRs are functional IRESs that bind to ribosomes, forming complexes that are predominantly in the P-site bound state. A second, weaker set of toeprints appeared on the NediV IRES +19–20 nt relative to $CCC_{1490–2}$ that may correspond to ribosomal complexes in which PKI is bound in the ribosomal E site or to partial unwinding of PKI in the P site. Equivalent +19–20 nt toeprints were barely apparent on the APLV1 IRES (Fig. 3B, lane 3).

Type 6a and type 6b IRESs bind to arthropod, mammalian and yeast ribosomes and function in various eukaryotic cells and cell-free extracts (Wilson et al. 2000a,b; Thompson et al. 2001; Nishiyama et al. 2003; Ruehle et al. 2015), and type 6c IRESs bind to mammalian and insect ribosomes to form elongation-competent complexes (Abaeva et al. 2020). We therefore also assayed binding of the NediV IRES to ribosomal subunits from the moth *Spodoptera frugiperda*. The IRES yielded toeprints predominantly +15–17 nt from $CCC_{1490–2}$ on binding to 80S ribosomes but not to 40S subunits alone (Fig. 3C).

## Elongation-competence of ribosomes assembled on NediV and APLV1 IRESs

NediV and APLV1 IRESs incubated with 40S subunits, Met-$tRNA_i^{Met}$ and eIFs did not form 48S complexes and therefore do not support initiation by the canonical mechanism (Fig. 3D,E). Inclusion of eEF1H and eEF2, aminoacylated tRNAs and cycloheximide with IRES-bound ribosomes enabled them to undergo one cycle of elongation, indicating that these complexes were elongation-competent (Fig. 3D, lane 7; Fig. 3E, lane 5). A −2 nt shift seen when 80S/IRES complexes were incubated with eEF2 alone (Fig. 3D, lane 6) may be due to changes in ribosome conformation caused by eEF2-mediated rotation (Flis et al. 2018; Susorov et al. 2018).

Elongation requires a vacant A site to which eEF1A can recruit aa-tRNA. In the CrPV IRES/80S complex, the A site becomes accessible to aa-tRNA only after eEF2-mediated translocation of PKI from it (Fernández et al. 2014). To test if ribosomal binding to NediV-like IRESs places the ORF2 start codons directly in the A site, we used IRES variants in which the NediV $GCU_{1493–5}$ and APLV1 $GCU_{5604–6}$ had been replaced by UCU (Ser) codons (chosen because Ser-$tRNA^{Ser}$ functions efficiently in in vitro reconstitution assays [Zinoviev et al. 2018]). A toeprint shift consistent with one cycle of elongation occurred in the presence of ribosomes, eEF1H, eEF2, and Ser-$tRNA^{Ser}$ (Fig. 3F,J). Binding of these IRESs to ribosomes therefore places the UCU triplet in the A site such that it can be decoded directly.

To confirm that the APLV1 GCU initiation codon is placed in the A site and is accessible, we used an IRES variant in which this codon was substituted by a UAA (stop) codon. eRF1 binds to the A site only when it contains a stop codon, inducing compaction of mRNA that is detected as a +1–2 nt toeprint shift (Alkalaeva et al. 2006; Muhs et al. 2015). Whereas binding of eRF1/eRF3 to an equivalent CrPV IRES variant required a prior eEF2-mediated translocation step, and therefore in the presence of eEF2 and eRF1/eRF3 yielded a stop that had shifted forward by +4 nt (Muhs et al. 2015), eRF1/eRF3 bound to ribosomes assembled on the mutated APLV1 IRES independently of eEF2, inducing a toeprint shift that corresponds to the expected compaction of mRNA in the A site (Fig. 3G, lane 3).

The bacterial toxin RelE specifically cleaves mRNA in the A site (Andreev et al. 2008; Neubauer et al. 2009) and can therefore also be used to assess this site's accessibility in

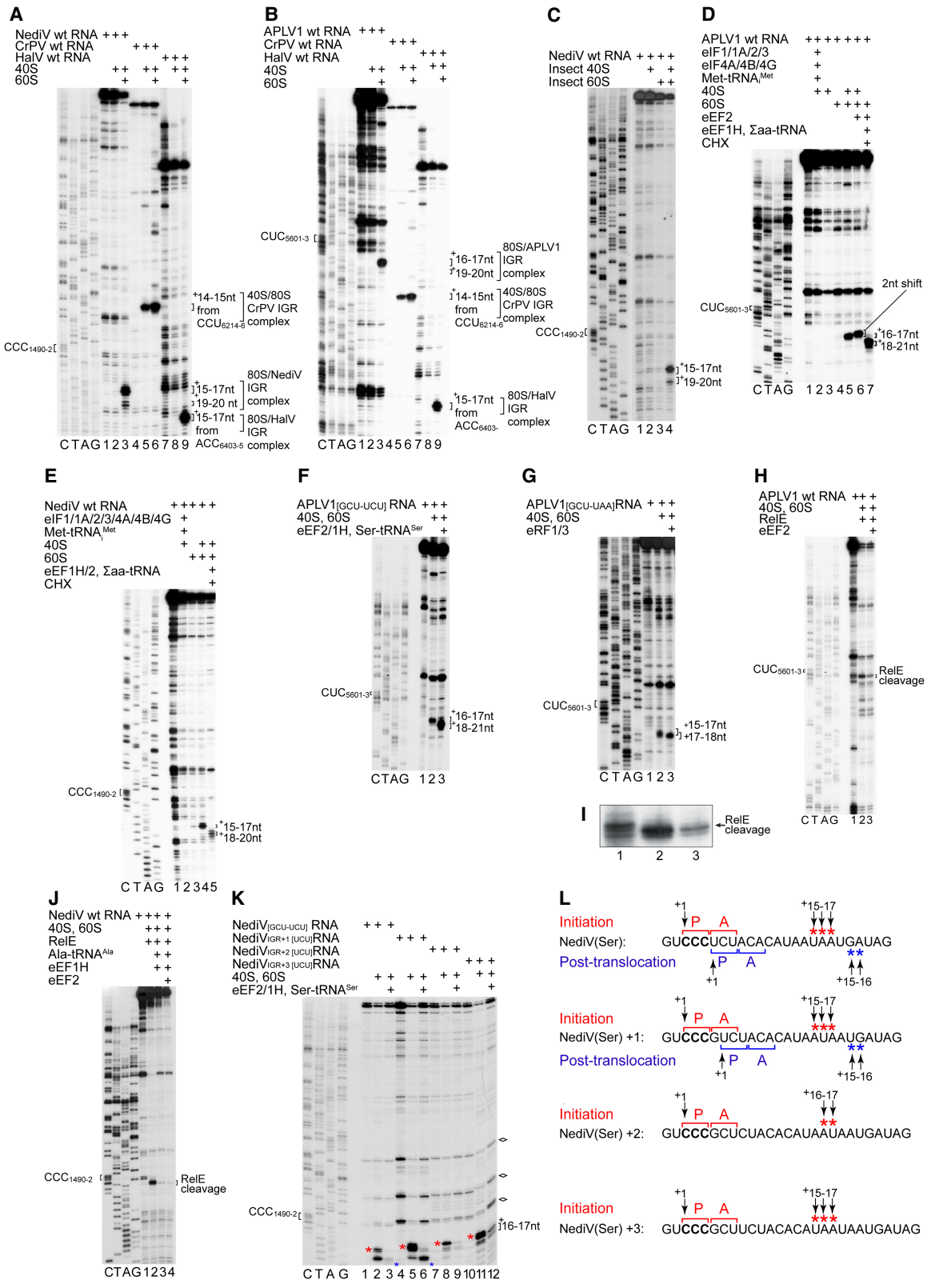


**FIGURE 3.** (Legend on next page)

IRES-bound ribosomal complexes. RelE cleaved APLV1 and NediV mRNAs at $GCU_{5604–6}$ and $GCU_{1493–5}$, respectively, indicating that these codons were in the A site and accessible in the absence of eEF2 (Fig. 3H–J). Inclusion of eEF2 or eEF1H/aa-tRNA inhibited RelE cleavage (Fig. 3H, lane 3; Fig. 3J, lanes 3,4; shown at higher resolution for APLV1 RNA in Fig. 3I), likely because these A-site ligands compete with RelE for access to the vacant A site. Taken together, these assays show that the A site in NediV-like IRES/80S initiation complexes is occupied by the ORF2 start codon and is accessible for decoding without prior eEF2-mediated translocation.

Type 6a, 6b and 6c IRESs can promote initiation in overlapping reading frames, resulting in translation of the ORF2 polyprotein (0 frame) and at a lower level, in the +1 frame (Ren et al. 2012; Petrov et al. 2016; Abaeva et al. 2020). To analyze the fidelity of reading frame selection on the NediV IRES, we used variants in which $GCU_{1493–5}$ had been substituted by UCU (Ser) codons in 0, +1, +2, or +3 positions (Fig. 3K,L). They all bound to ribosomes, but only the 0 and +1 frame variants supported elongation in the presence of eEF1H, eEF2, and Ser-$tRNA^{Ser}$. The NediV IRES can therefore initiate translation in 0 and +1 reading frames. In these experiments, the separation between the UCU (Ser) codon and the primer binding site used for toeprinting of complexes assembled on different mRNAs is constant even as the separation between the UCU codon and the P-site $CCC_{1490–2}$ codon changes, so that IRES-bound ribosomes that undergo a single cycle of elongation in 0 or +1 reading frames will yield a toeprint at the same position. However, the insertion of nucleotides upstream of the UCU (Ser) codon leads to a progressively increasing separation between it and endogenous sites of RT arrest, such as at the junction of S3.1 and helix P1.3 (Fig. 3K).

The NediV IRES mutant with a UCU (Ser) codon located two triplets downstream from the CCC triplet in PKI yielded toeprints consistent with its binding in the P site and +19–20 nt toeprints that might reflect destabilization of the IRES or binding in the E site (Fig. 3K, lane 11). The putative E-site bound fraction of these complexes did not recruit Ser-$tRNA^{Ser}$ to the A-site UCU codon and undergo subsequent eEF2-mediated translocation, suggesting that if PKI does bind in the E site, the resulting IRES/80S complexes are not competent to begin elongation.

## SERBP1/eEF2 inhibit binding of NediV and APLV1 IRESs to ribosomes

Although NediV-like IGR IRESs initiate translation efficiently in in vitro reconstituted reactions, the NediV IRES did not promote translation when added to rabbit reticulocyte lysate (RRL) (Fig. 3A, lane 3). ORF2 translation was apparent after preincubation of the IRES with salt-washed 40S and 60S subunits (Fig. 3A, lane 5), suggesting either that the addition of purified ribosomes compensates for these IRES having low affinity for ribosomes, or that endogenous ribosomes are bound by an inhibitory factor that is removed by salt-washing. Native ribosomes purified from RRL are associated with eEF2 and SERPINE1 mRNA binding protein 1 (SERBP1) (Zinoviev et al. 2015; Brown et al. 2018; Abaeva et al. 2020), and in contrast to ribosomes reassembled from salt-washed subunits, do not bind to the type 6c (Abaeva et al. 2020) or to NediV IGR IRESs (Fig. 4C, lane 6). SERBP1 binds to the head of the 40S subunit and to the mRNA-binding channel, where it interacts

**FIGURE 3.** The mechanism of initiation on type 6d IRESs. (*A*,*B*) Assembly of ribosomes from 40S and 60S subunits on (*A*) NediV, (*B*) APLV1 and (*A*, *B*) CrPV and HalV IRESs, assayed by toeprinting. The NediV $CCC_{1490–2}$ and APLV1 $CUC_{5601–3}$ triplets that precede ORF2 are indicated on the *left* and the positions of toeprints relative to these codons are indicated on the *right* of panels *A–K*. (*A*) The +15–17 nt toeprints on the *right* correspond to binding of NediV $CCC_{1490–2}$ in the P site of IRES-bound ribosomes; the +19–20 toeprints are discussed in the text. (*B*) The +16–17 nt toeprints on the *right* correspond to binding of APLV1 $CUC_{5601–3}$ in the P site of IRES-bound ribosomes, analogously to the toeprints +14–15 nt from CrPV $CCU_{6214–6}$ and +15–17 nt from HalV $ACC_{6403–5}$. (*C*) Assembly of *S. frugiperda* ribosomes on the NediV IRES, assayed by toeprinting. (*D–F*) Toeprinting analysis of ribosome assembly and subsequent elongation on (*D*) APLV1 wt, (*E*) NediV wt, and (*F*) $APLV1_{[GCU\text{-}UCU]}$ mutant mRNAs incubated with ribosomal subunits with (*D*,*E*) or without (*F*) canonical eIFs and Met-$tRNA_i^{Met}$ and with (*D*,*E*) eEF1H/2, ∑aa-tRNA and cycloheximide (CHX) or (*F*) eEF1H/2 and Ser-$tRNA^{Ser}$. The shifts in toeprints (*D*) caused by eEF2 alone and (*D–F*) after the first cycle of elongation are indicated on the *right* of each panel. (*G*) A-site accessibility in 80S:IRES binary complexes analyzed by binding eRF1/eRF3 and eEF2 to $APLV1_{[GCU\text{-}UAA]}$ mRNA, assayed by toeprinting. The positions of toeprints relative to the P site codon $CUC_{5601–3}$ are indicated on the *right*. (*H–J*) A-site accessibility in 80S complexes assembled on (*H*,*I*) APLV1 and (*J*) NediV IRESs, assayed by RelE cleavage. RelE cleavage of the APLV1 IRES in (*H*) is shown at high resolution in (*I*). Sites of cleavage are indicated on the *right*. (*K*,*L*) The fidelity of reading frame selection investigated by the ability of 80S complexes formed on the NediV IRES with (*K*) a UCU (Ser) codon in the 0 reading frame or placed in the +1, +2, or +3 reading frames by inserting G, GC, and GCT nucleotides, respectively, between $CCC_{1490–1492}$ and $UCU_{1493–1495}$ (Ser) codons to undergo a single cycle of elongation in presence of Ser-$tRNA^{Ser}$, eEF1H/2, and ribosomal subunits, assayed by toeprinting. Stops induced by initiation and post-translocation 80S ribosomes are indicated by red and blue asterisks, respectively. RT stops induced by structured RNA elements independently of ribosomes are marked with diamonds on the *right*. (*L*) The initiation codon (bold) and flanking nucleotide sequences of $NediV_{[UCU]}$, $NediV_{IGR\,+\,1[UCU]}$, $NediV_{IGR\,+\,2[UCU]}$ and $NediV_{IGR\,+\,3[UCU]}$ mRNAs annotated to show the P site and A site codons in 80S initiation and post-translocation complexes *above* and *below* individual mRNA sequences, together with the +1 nt in the P site of pretranslocation complexes, and the toeprints from 80S initiation and post-translocation complexes (red and blue asterisks, as in panel *K above* and *below* individual mRNA sequences). Panel *L* summarizes data from panel *K*. (*A–K*) Lanes C, T, A, G show dideoxynucleotide sequence of (*A*,*C*,*E*,*I*,*J*,*K*) NediV and (*B*,*D*,*F*,*G*,*H*) APLV1 mRNAs generated with the same primer as in toeprinting assays. Positions of P sites ($CCC_{1490–2}$ and $CUC_{5601–3}$ for NediV and APLV1, respectively) and 80S:IRES complexes are indicated. (*C*,*D*) Separation of lanes by white lines indicates that they were juxtaposed from the same gel.

with eEF2 in the A site (Brown et al. 2018). In vitro, SERBP1 and eEF2 inhibited 80S complex formation on NediV (Fig. 4C, lane 5) and APLV1 (Fig. 4D, lane 5) IRESs, on the type 6c HalV IRES, but not on the type 6a CrPV IRES (Fig. 4E; Abaeva et al. 2020). SERBP1 alone weakly inhibited binding of the APLV1 IRES to ribosomes and had little effect on binding of the NediV IRES (Fig. 4D, lane 4; Fig. 4E, lane 4).

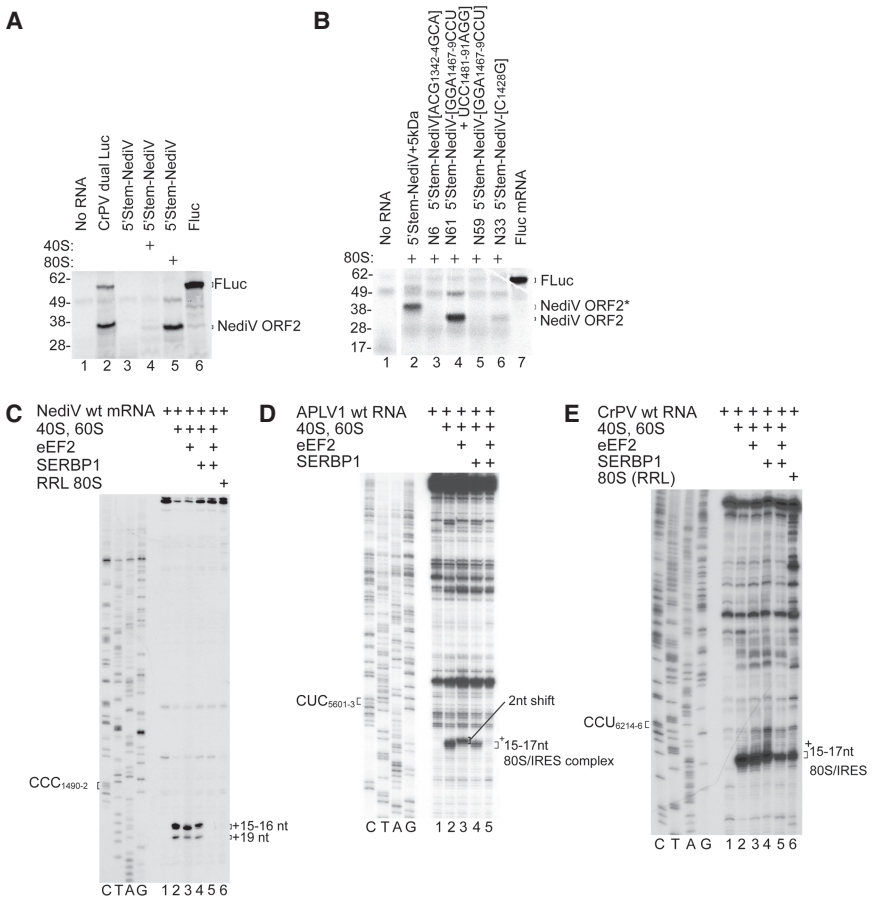


**FIGURE 4.** Inhibition of NediV IGR IRES function by SERBP1/eEF2. (*A*,*B*) Translation of 5′-stem-NediV IRES mRNAs in RRL with or without preincubation with purified 40S subunits or 80S ribosomes. (*A*) FLuc and CrPV dual Luc mRNAs are positive controls. The FLuc and NediV ORF2 translation products are indicated on the *right* and molecular weight markers (kDa) on the *left*. (*B*) Translation of 5′-stem-NediV IRES + 5 kDa and mutant versions of 5′-stem-NediV IRES mRNA with substitutions in IRES domain 1 (N6), domain 2 (N33), and domain 3 (N59 and N61), after preincubation with 80S ribosomes. FLuc mRNA was a positive control. The FLuc, NediV ORF2, and NediV-(ORF2 + 5 kDa) translation products are indicated on the *right* and molecular weight markers (kDa) on the *left*. (*C*) Influence of SERBP1 and eEF2 on binding of ribosomes to the NediV IRES, assayed by toeprinting. The positions of +16–+17 nt and +19 nt toeprints are shown on the *right*. Lanes C, T, A, G depict the NediV sequence. (*D*,*E*) Influence of SERBP1 and eEF2 on ribosomal complex formation on (*D*) APLV1 and (*E*) CrPV IRESs incubated with SERBP1, eEF2, and ribosomal subunits or native ribosomes, as indicated. The positions of the P-site codon and of ribosomal complexes are indicated on the *left* and on the *right* of gel panels, respectively. Lanes C, T, A, and G show (*D*) APLV1 and (*E*) CrPV sequences, respectively. (*B*) Separation of lanes by white lines indicates that they were juxtaposed from the same gel.

## Domain 1 contains important determinants of ribosomal binding

We used toeprinting to assay the ribosome-binding activity of mutant forms of NediV and APLV1 IRESs to validate the structural models (Fig. 2B,C) and to relate structure to mechanism. The ORF1 coding sequence was not required but 5′-terminal deletion to APLV1 nt 5459 and to NediV nt 1343 or 1351 reduced ribosomal binding (Fig. 5A, lanes 2,4,7,10; Fig. 5C, lanes 2,4,7). P1.1, L1.1 and P1.2 elements are therefore functionally important and P1.1 forms the 5′ border of these IRESs.

The L1.1a and L1.1b loops in NediV-like IRESs contain conserved AUACG and G(U/A)CAGG motifs, respectively (Fig. 2A), that differ from analogous conserved elements in type 6a, 6b, and 6c IRESs that interact with the L1 stalk of the 60S subunit (Schüler et al. 2006; Koh et al. 2014; Abaeva et al. 2020). Toeprinting assays showed that substitutions in them strongly impaired ribosomal binding to the APLV1 IRES (Fig. 5D, mutants A3–A6) and reduced binding to the NediV IRES (Fig. 5E, mutants N5–N8). Consistently, binding of NediV mutant N6 to 80S ribosomes in sucrose-density gradient (SDG) centrifugation experiments was strongly reduced (Fig. 5B) and translational activity in RRL after incubation of mutant mRNA with 80S ribosomes was abrogated (Fig. 4B, lane 3). The L1.1a and L1.1b loops are therefore key determinants of IRES function.

Ribosome binding was impaired by disruptive substitutions in APLV1 P1.1, P1.2, and P1.3 and in NediV P1.2 and P1.3 but was partly or wholly restored by second-site substitutions (Fig. 5D, mutants A1–A2, A7–A18; Fig. 5E, mutants N9–N18). Restoration of ribosome-binding activity by compensatory substitutions indicates that the function of these elements is structural rather than sequence-specific.

## Domain 2 promotes stable binding of PKI in the ribosomal P site

Domain 2 is a conserved structural component of type 6d IRESs that differs significantly from domain 2 in type 6a

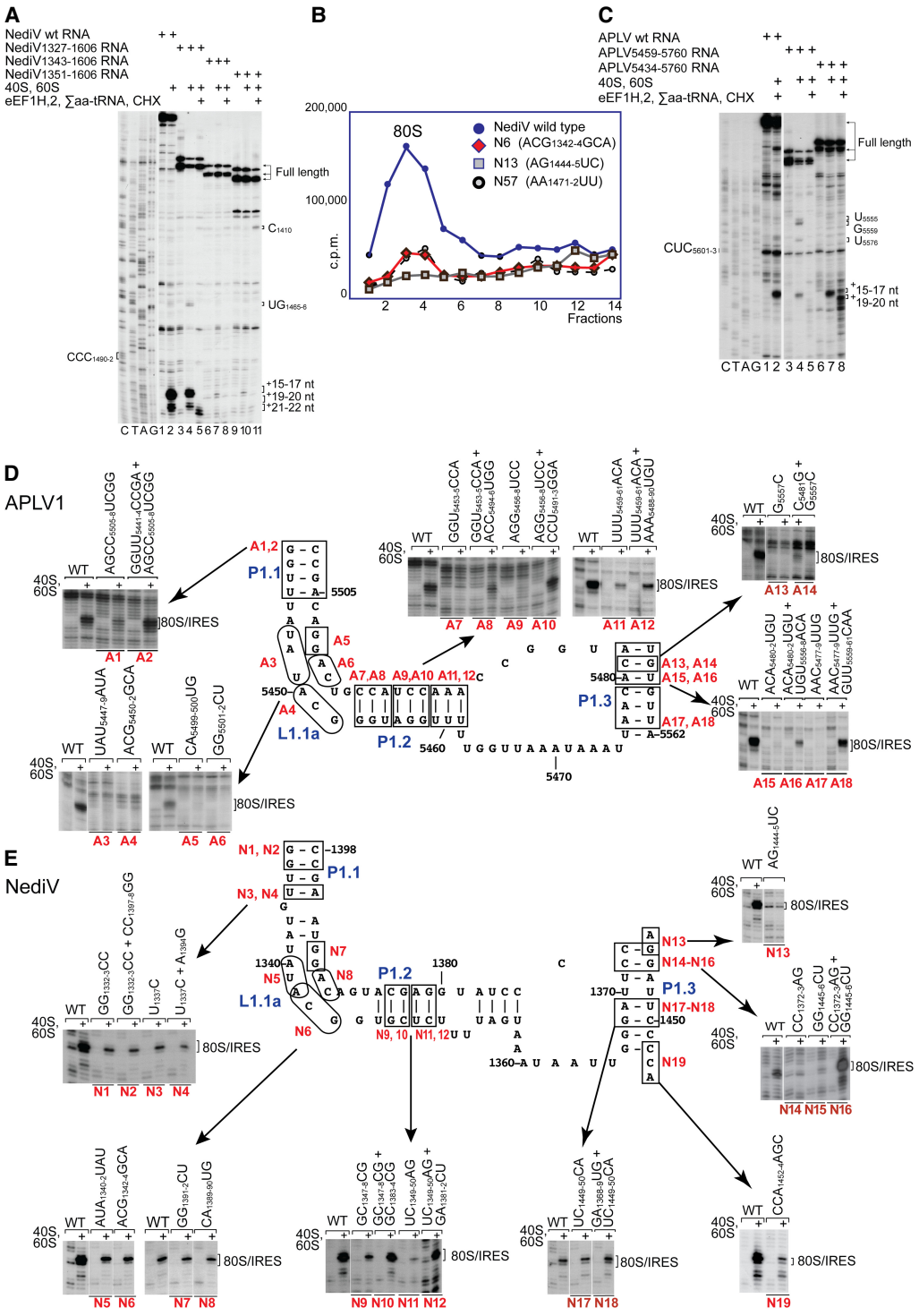


**FIGURE 5.** Mutational analysis of domain 1/PKII. (*A*,*C*) Toeprinting analysis of the influence of 5′-terminal deletions of (*A*) the NediV IRES and (*B*) the APLV1 IRES on their ability to support binding of ribosomes and subsequent elongation upon inclusion of the indicated components. The positions of the codons that occur immediately upstream of ORF2 coding sequences are indicated on the *left*, and full-length cDNAs and toeprints from ribosomal complexes before and after elongation are indicated on the *right*. Lanes C, T, A, G depict (*A*) NediV and (*C*) APLV1 sequences. (*B*) Association of $^{32}$P-labeled wt and mutant NediV IGR-containing mRNAs with 80S ribosomes, assayed by sucrose density gradient centrifugation. Mutant mRNAs had substitutions in domain 1 (N6, N13) or in domain 3 (N57). Sedimentation was from *right* to *left*, and the position of 80S complexes is indicated. Fractions from the upper part of the sucrose gradient have been omitted for greater clarity. (*D*,*E*) The influence of disruptive and compensatory substitutions in P1.1, P1.2, and P1.3 helices and the L1.1 loop of (*D*) APLV1 and (*E*) NediV IRESs, as indicated on the models of IRES domain 1. IRES activity in ribosomal binding was assayed by toeprinting. The positions of 80S:IRES complexes are indicated on the *right* of each panel. (*A*,*C*–*E*) Separation of lanes by white lines indicates that they were juxtaposed from the same gel.

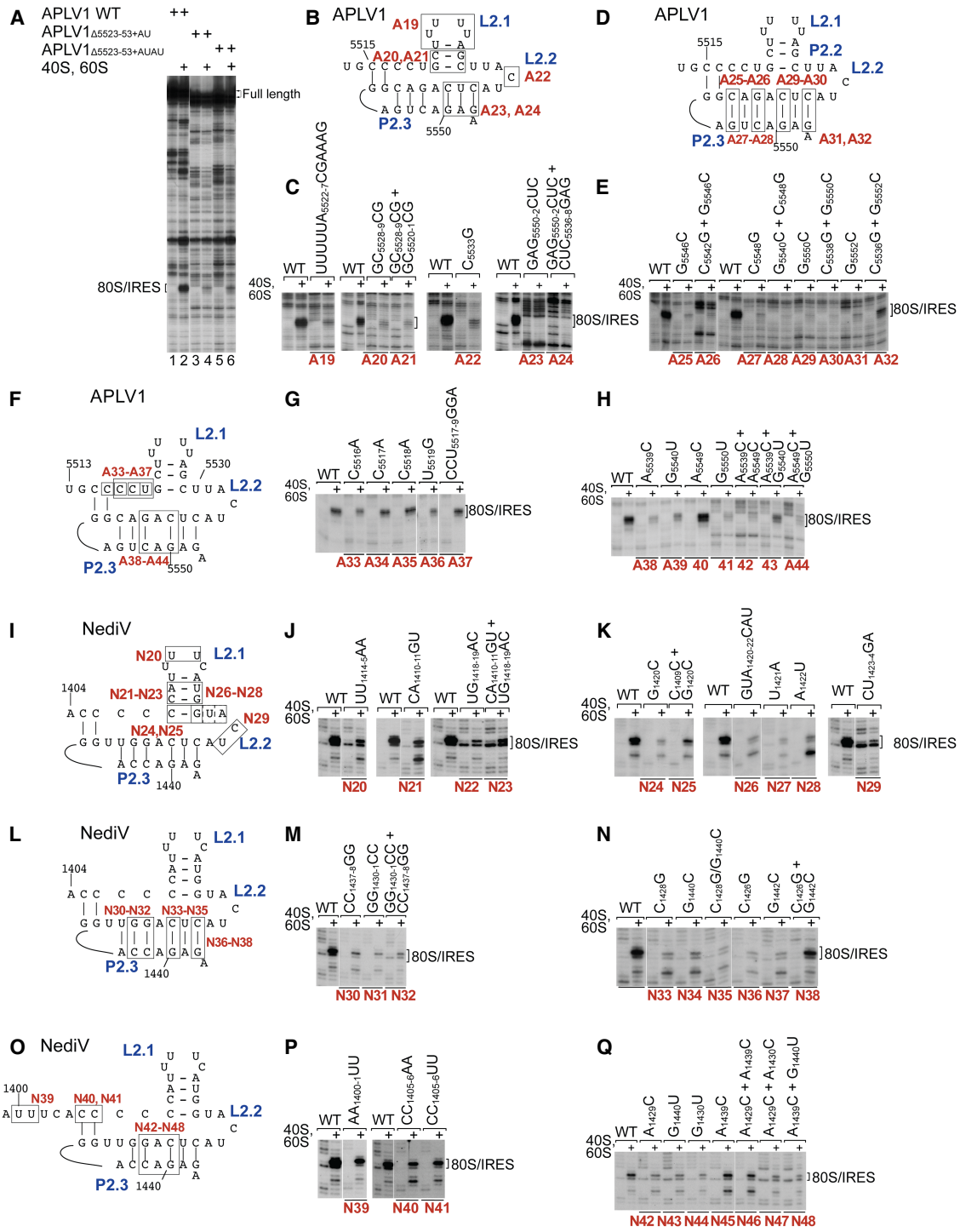


**FIGURE 6.** Mutational analysis of domain 2/PKIII. (*A*) Influence of APLV1 PKIII deletion on 80S:IRES complex formation, assayed by toeprinting. The influence of disruptive or compensatory substitutions in domain 2 of (*B–H*) the APLV1 IRES and (*I–Q*) the NediV IRES on binding of ribosomes, assayed by toeprinting. (*A–H*) Separation of lanes by white lines indicates that they were juxtaposed from the same gel. Positions of 80S:IRES complexes are indicated on the *left* (*A*) or *right* (*C–Q*).

IRESs. Deletion analysis suggested that APLV1 stem–loops P2.2/L2.1, P2.3/L2.2, and P2.4/L2.3 are important for function (Fig. 6A). The most sensitive region was P2.4: toeprinting showed that all mutations in it strongly reduced the ability of the IRES to insert stably into the ribosomal mRNA-binding cleft (Fig. 6C,E,H,M,N,Q), and that full activity was restored by compensatory substitutions at only one base-pair in this element, at the base of P2.4 (APLV1

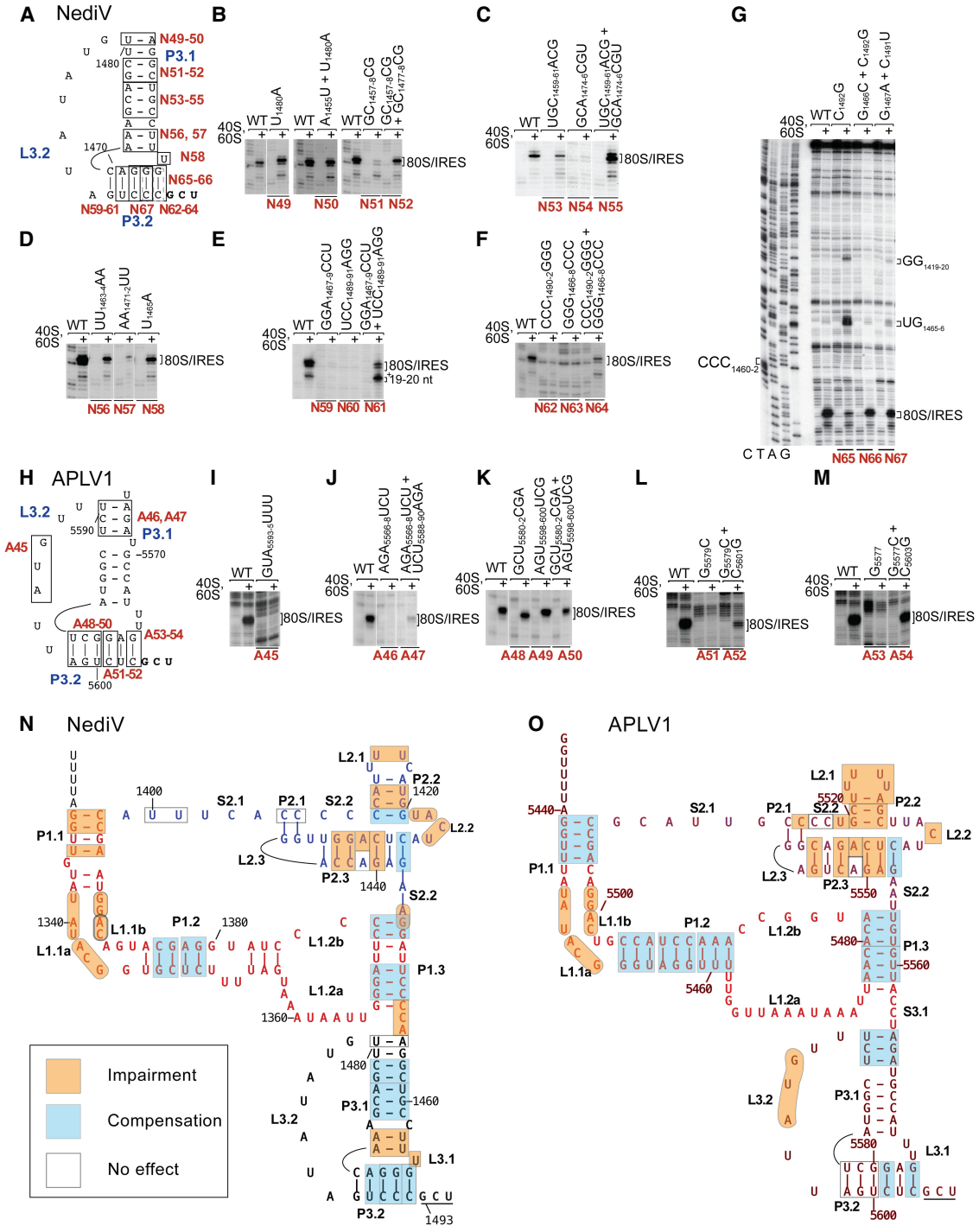


**FIGURE 7.** Mutational analysis of domain 3/PKI. The influence of disruptive or compensatory substitutions in domain 3 of (*A–G,N*) the NediV IRES and (*H–M,O*) the APLV1 IRES on binding of ribosomes, assayed by toeprinting. Separation of lanes by white lines indicates that they were juxtaposed from the same gel. Positions of 80S:IRES complexes are indicated on the *right*. Summary of the effects of substitutions in (*N*) NediV and (*O*) APLV1 IRESs. Models of these IRESs are annotated to show mutations that (a) have no effect, (b) cause loss of function that is compensated by second-site mutations, and (c) impair function or lead to loss of function that is not compensated by second-site mutations, as indicated in the *inset* key.

$C_{5536}$–$G_{5552}$ and NediV $C_{1426}$–$G_{1442}$) (Fig. 6E, mutant A32; Fig. 6N, mutant N38). The failure of second-site substitutions to restore ribosome-binding activity suggests that conserved elements in this domain determine functionally important aspects of higher-order structure. Notably, several substitutions strongly increased the proportion of

toeprints appearing +19–20 nt from $CCC_{1490–2}$ relative to those at +15–17 nt, for example in NediV mutants N21 (Fig. 6J), N26, N28 (Fig. 6K), N33, N34, and N37 (Fig. 6N). The translational activity in RRL of a representative mutant NediV mRNA (N33) that had been preincubated with 80S ribosomes was strongly reduced by destabilization of P2.3 by the $C_{1428}G$ substitution (Fig. 4B, lane 6).

Additional RT stops appear at $UG_{1465–6}$ in domain 1 and at $C_{1410}$ and $GG_{1419–20}$ in domain 2 on incubation of ribosomes with some NediV IRES mutants (e.g., Fig. 5A, lanes 4,5,11; Fig. 7G, lanes 4,8). Similar stops appeared on incubation of ribosomes with APLV1 IRES mutants (Fig. 5C, lane 4). These stops resemble ribosome-induced stops that appeared in L3.1 and domain 2 of the type 6a CrPV IRES and in P3.2 of the type 6b TSV IRES (Wilson et al. 2000a; Pestova et al. 2004; Jang and Jan 2010; Muhs et al. 2015) and are likely caused by IRES-ribosome contacts that are detectable only when binding of PKI in the mRNA-binding channel fails to arrest reverse transcription. Domain 2 therefore functions to ensure stable binding of domain 3 (PKI) in the P site.

## Structural determinants of function in domain 3

In all IGR IRESs, domain 3, which consists of PKI and the L3.2 variable loop region (VLR), mimics the tRNA ASL base-paired via its anticodon to mRNA. Disruption of helical regions reduced the intensity of toeprints that are indicative of stable binding by NediV and APLV1 IRESs in the mRNA-binding cleft, but binding activity was partly or fully restored by second-site substitutions (e.g., Fig. 7B, mutants N51, N52; Fig. 7C, mutants N54, N55; Fig. 7E, mutants N60, N61; Fig. 7L, mutants A51, A52; Fig. 7M, mutants A53, A54) albeit in some instances only weakly (Fig. 7F, mutants A62–A64; Fig. 7J, mutants A46, A47) (summarized in Fig. 7N,O). Consistently, binding of NediV mutant N57 to 80S ribosomes in SDG centrifugation experiments was strongly reduced (Fig. 5B) and translational activity in RRL after incubation of mutant mRNA with 80S ribosomes was abrogated as a consequence of the destabilization in mutant N59 but was restored by compensatory substitutions in mutant N61 (Fig. 4B, lanes 4,5).

The requirement for base-pairing was particularly pronounced for P3.2 in the NediV IRES, and although binding activity (assayed by toeprinting) was restored by compensatory substitutions, the intensity of toeprints at +19–20 nt relative to those at +15–17 nt was greater for some double mutants than for the wt IRES (e.g., Fig. 7E, mutant N61; Fig. 7F, mutant N64). Association of the IRES with the ribosomal mRNA-binding cleft was impaired by substitutions in APLV1 L3.2 (Fig. 7I, mutant A45). Destabilizing substitutions in the half of APLV1 P3.2 that is adjacent to the GCU initiation codon impaired ribosomal binding to the P site to a greater extent than substitutions in the distal half (compare mutant A51 [Fig. 7L] and mutant A53 [Fig. 7M] with mutants A48–A49 [Fig. 7K]; summarized in Fig. 6O).

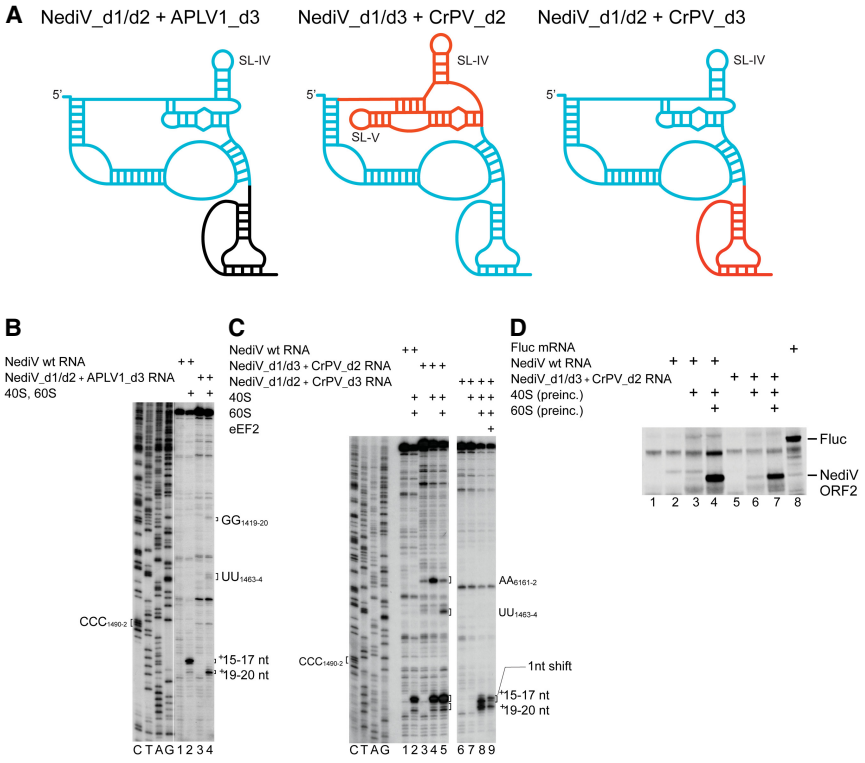


**FIGURE 8.** 80S complex formation on chimeric NediV/APLV1 and NediV/CrPV IRESs. (*A*) Schematic models of hybrid IRESs. Elements derived from NediV, APLV1, and CrPV IRESs are colored light blue, black, and red, respectively. (*B*) Binding of ribosomes to NediV wt and NediV/APLV1 chimeric IRESs, assayed by toeprinting. Separation of lanes by white lines indicates that they were juxtaposed from the same gel. (*C*) Binding of 40S or 40S and 60S subunits to NediV wt and NediV/CrPV chimeric IRESs, followed by elongation on inclusion of eEF1H/2H, ∑aa-tRNA, and cycloheximide (CHX), assayed by toeprinting. (*B*,*C*) Positions of the P site codon and of bound ribosomal complexes are indicated. Lanes C, T, A, G depict NediV sequence.

## Activity of hybrid NediV/APLV1 and NediV/CrPV IGR IRESs

We created a panel of chimeric IRESs to gain further insight into the functions of the domains of NediV-like IGR IRESs (Fig. 8A). Whereas the NediV wt IRES yielded toeprints predominantly at +15–17 nt from

$CCC_{1490–2}$, the NediV[d1/d2] + APLV1[d3] chimera, in which APLV1 domain 3 replaced NediV domain 3, yielded toeprints exclusively at +19–20 nt (Fig. 8B, lanes 2,4). Domain exchange constitutes an extreme example of nucleotide substitutions that altered the positioning or stability of this domain on the ribosome.

Substitution of NediV domain 2 by CrPV domain 2 (nt 6096–6132) yielded the chimeric NediV[d1/d3] + CrPV [d2] IRES that bound 40S subunits directly, leading to the appearance of toeprints at +15–17 nt and to a lesser extent at +19–20 nt (Fig. 7C, lane 4). The appearance of these two sets of toeprints suggests that although the IRES binds preferentially to the P site of the 40S subunit, domain 3 may have bound to the E site or have been partially destabilized in a subset of the resulting complexes. IRES/40S complexes also yielded toeprints at $AA_{6161–2}$ in CrPV domain 2, as noted previously for the wt CrPV IRES (Wilson et al. 2000a). Inclusion of 60S subunits in assembly reactions led to the prominent appearance of additional toeprints at $UU_{1463–4}$ which correspond to toeprints seen on binding of ribosomes to the NediV [d1/d2] + APLV1[d3] chimera (Fig. 8B, lane 4) and at $G_{6183}$ following joining of a 60S subunit to the 40S/CrPV IRES complex (Wilson et al. 2000a). Although toeprinting showed that this chimeric IRES was bound stably in the ribosomal P site, it did not support translation in RRL unless the chimeric mRNA had been preincubated with 80S ribosomes, and to a much lesser extent, with 40S subunits (Fig. 8D, lanes 5–7).

A chimeric NediV[d1/d2] + CrPV[d3] IRES was unable to bind 40S subunits, but did bind 80S ribosomes, yielding two sets of toeprints (Fig. 8C, lanes 7–9). They appeared 2 nt downstream compared to those from ribosomes bound to the wt NediV IRES, a difference that reflects the slightly larger domain 3 in the CrPV IRES. Inclusion of eEF2 with 40S and 60S subunits induced a 1 nt reverse shift in the toeprints at +15–17 nt (Fig. 8C, lane 9), similar to that noted earlier for the NediV IRES (Fig. 3D, lane 6). It remains to be determined whether this mutant mRNA was active in promoting translation in RRL.

## DISCUSSION

### Structural characteristics of type 6d IGR IRESs

NediV and APLV1 exemplify a group of IRESs, here designated type 6d, that shares some properties with the well-characterized type 6a IRESs (e.g., CrPV) and type 6b IRESs (e.g., TSV), and the recently identified type 6c IRESs (e.g., HalV). They all initiate from non-AUG codons without the involvement of Met-$tRNA_i^{Met}$ or initiation factors by binding directly to the ribosome, and they all contain a pseudoknot (PKI) that mimics the tRNA ASL-mRNA interaction (Schüler et al. 2006; Costantino et al. 2008; Abaeva et al. 2020).

These similarities are striking, but there are significant differences between type 6d and other IGR IRES classes (Fig. 1). Although they resemble type 6a and 6b IRESs in having a three-domain structure that contains three pseudoknots, type 6d IRESs are only ∼165 nt long and are thus substantially smaller than these classes. Some helical regions in type 6d IRESs are shorter than in their counterparts, L1.1a and L1.1b loops in domain 1 lack sequence motifs that are conserved in type 6a and 6b IRESs, and PKIII (domain 2) has a distinctive structure. It contains a strongly conserved loop motif (L2.2) that does not occur in type 6a or 6b IRESs and lacks an equivalent of SLV (which in type 6a and 6b IRESs binds to the head of the 40S subunit and is important for IRES function [Jan and Sarnow 2002; Nishiyama et al. 2003; Schüler et al. 2006; Fernández et al. 2014]). The widespread restoration of type 6d IRES function by second-site substitutions that reestablish base-pairing indicates that most (but not all) helices have structural rather than sequence-specific roles. The failure of some second-site substitutions in domain 2 and in helix P3.2 to restore function despite restoration of the potential for base-pairing suggests that specific structural or mechanical consequences of base-pairing in these helical elements are important for function. Nucleotide sequence determines structural properties of RNA helices such as the width of the major groove, bending and engagement in tertiary interactions, and influences mechanical properties such as flexibility (e.g., Šponer et al. 2018; Yesselman et al. 2019). These properties could all influence whether the IRES engages productively with the ribosome. Taken together, the present report and the recent identification of the type 6c IRES (Abaeva et al. 2020) indicate that IGR IRESs are unexpectedly diverse.

### The mechanism of initiation on type 6d IRESs

The structural similarities and differences between type 6d and the other classes of IGR IRES parallel similarities and differences between the mechanisms by which they promote initiation. Type 6d IRESs bind directly to mammalian and insect ribosomes (Fig. 3A–C) and thus like type 6a, 6b, and 6c IRESs, likely engage with conserved elements of the eukaryotic ribosome. In contrast to type 6a and 6b IRESs, but like type 6c IRESs, they do not bind stably to 40S subunits (Figs. 3A,B), suggesting that their divergent domain 2 does not engage strongly with this subunit, and that the interaction of domain 3 with the P site is not sufficient for stable binding to the 40S subunit in the absence of stabilizing IRES-60S subunit interactions. Notably, substitution of NediV domain 2 by CrPV domain 2 is sufficient to confer the ability on the resulting chimeric IRES to bind directly and stably to 40S subunits (Fig. 8C).

A major difference between type 6d IRESs and both type 6a and type 6b IRESs is that domain 2 in the former

lacks an equivalent of SLV. This stem–loop binds to rpS25 in the head of the 40S subunit (Muhs et al. 2011) and is an important determinant of function in type 6a IRESs (Jan and Sarnow 2002; Nishiyama et al. 2007), so that the absence of an analogous element in type 6d IRESs (Fig. 2) is at first sight surprising. However, there may be an overlap in the function (and consequent redundancy) between SLV and the adjacent SLIV in stabilizing binding of the IRES to the 40S subunit (Kerr et al. 2016). Moreover, mutations that strongly impaired the function of SLV in supporting IRES-mediated translation in vitro have marginal effects on viral multiplication, suggesting that cellular conditions may be altered during infection to suppress defects in IRES function (Kerr et al. 2016). Possible changes include modification of elements of the translation apparatus such as the ribosome or of proteins that bind to it and modulate its activity. We have previously suggested (Abaeva et al. 2020) that the activity of IRESs may be enhanced during viral infection by changes that result in dissociation from ribosomes of hibernation factors such as IFRD2 or Serbp1 and eEF2 that sequester them in an inactive state (Zinoviev et al. 2015; Brown et al. 2018). Their association with hibernating ribosomes is regulated by signaling pathways (Smith et al. 2021; Shetty et al. 2023) that could potentially be activated as a result of dicistrovirus infection, thereby promoting dissociation of hibernation factors from ribosomes. Although the inability of the NediV IRES to promote translation in RRL without preincubation with 80S ribosomes may reflect a low affinity for ribosomes, it is also likely that initiation on type 6c and 6d IRESs is particularly sensitive to processes that modulate sequestration of 80S ribosomes because initiation occurs by direct binding to 80S ribosomes rather than to 40S subunits and the number of vacant 80S ribosomes in cells is low.

Mutational analysis yielded insights into the importance of specific elements in type 6d IRESs. The sequence conservation of the L1.1 loop (Fig. 2A), the weakening of ribosomal binding to NediV and APLV1 IRESs caused by substitutions in it, and the resulting loss of function in supporting in vitro translation (Fig. 4B) indicate that this element is functionally important, likely by contributing to the interaction with the 60S subunit, as for type 6a IGR IRESs (Pfingsten et al. 2006, 2010). Whether this loop interacts with the P1 stalk in a similar manner to analogous elements in type 6a, 6b, and 6c IRESs (Schüler et al. 2006; Koh et al. 2014; Abaeva et al. 2020) despite the sequence differences remains to be determined.

The appearance of weak toeprints at +19–20 nt on binding of the NediV IRES to ribosomes in addition to the +15–17 nt toeprints could be due to binding of PKI to the E site in a fraction of these complexes, either directly or by spontaneous translocation from the P site, or reflect stochastic destabilization of PKI after binding to the P site. Spontaneous translocation of PKI between A and P sites and possibly from P to E sites has been noted for the CrPV IRES (Yamamoto et al. 2007; Muhs et al. 2015; Petrov et al. 2016; Pisareva et al. 2018), as has destabilization of PKI of the HalV IRES in the P site of the ribosome in the rotated state (Abaeva et al. 2020) and more extensively, of the CrPV IRES following translocation to the E site (Pisareva et al. 2018). Further investigation of the requirements for translocation of NediV-like IRESs and of possible structural changes in them during this process is needed to distinguish between these possibilities, and to determine whether the enhanced appearance of +19–20 nt toeprints following mutation of domain 2 reflects loss of the ability to establish interactions that retain PK1 in the P site or a reduction in rigidity that facilitates destabilization.

Type 6a and type 6b IRESs initially bind to the ribosome such that PKI is in the A site and must undergo eEF2-mediated translocation to the P site for translation to commence, whereas type 6d IRESs resemble type 6c IRESs (Abaeva et al. 2020) in binding such that PKI predominantly occupies the P site, leaving the A site vacant so that it can accept a cognate aa-tRNA without the need for a prior pseudotranslocation step. The resulting complex can engage eEF2 to promote translocation of the aa-tRNA from A to P sites and PKI from P to E sites, after which the vacated A site is again able to accept a cognate aa-tRNA, leading to peptide bond formation and further productive elongation cycles.

Like type 6a (Petrov et al. 2016; Kerr et al. 2018), 6b (Ren et al. 2012), and 6c (Abaeva et al. 2020) IRESs, the type 6d IRESs described here are not completely specific in their choice of reading frame and can promote initiation in the +1 frame (Fig. 3K). However, whereas the ORFs in the +1 reading frames of Israeli acute paralysis virus and cricket paralysis virus encode 94 and 41 a.a.-long polypeptides, respectively, that in the latter case contribute to pathogenesis (Ren et al. 2012; Kerr et al. 2018), the +1 reading frames in the NediV and APLV1 genomes immediately downstream from their IGR IRESs contain much shorter ORFs that encode 7 a.a.-long oligopeptides. Out-of-frame initiation mediated by the CrPV IRES appears to occur by two distinct mechanisms, involving either the entry of IRES-proximal codons in 0 or +1 frames into the A site (Petrov et al. 2016), or an ill-defined process of repositioning of ribosomes so that a codon 38–41 nt downstream from the IRES-adjacent GCU codon enters the A site (Kerr et al. 2018). In the first case, selection of the reading frame on the CrPV IRES occurs as a consequence of binding of the first aminoacyl-tRNA (Petrov et al. 2016), indicating that the appearance of a codon in the +1 frame in the A site occurs during or after translocation of PKI from A to P sites. In the case of HalV (Abaeva et al. 2020) and NediV (this report), entry of a codon into the A site must occur concurrently with binding of PKI in the P site. The experiments reported here for NediV and elsewhere for HalV (Abaeva et al. 2020) included a single species of aminoacyl-tRNA in in vitro reconstituted reactions and therefore minimized variables that can influence the

utilization of alternate reading frames such as the simultaneous presence in the reaction milieu of aa-tRNAs corresponding to both 0 and +1 codons. Nevertheless, the significant level of out-of-frame initiation that occurs in these conditions emphasizes that it reflects a fundamental property of type 6c and 6d IRESs. The lack of specificity in reading frame selection is thus characteristic of all IGR IRES classes and likely reflects the influence of shared structural properties on the presentation of alternate codons in the A site. These properties may include the potential for base-pairing involving the +1 nucleotide of the codon adjacent to PKI (Ren et al. 2012), the absence of modified nucleotides in PKI, differences between the interactions of PKI and of aa-tRNA with the ribosomal P site, and the dynamic nature of the P3.2 helix in PKI (Pisareva et al. 2018; Abaeva et al. 2020).

## MATERIALS AND METHODS

### Sequences

Sequences from the NCBI database (http://www.ncbi.nlm.nih.gov/nuccore) had the following accession numbers: Antarctic picorna-like virus 1 (APLV1, KM259869.1); Beihai picorna-like virus 78 (KX883307.1), Changjiang picorna-like virus 9 (KX884541.1); cricket paralysis virus (CrPV, NC_003924.1); *Gingko biloba* dicistrovirus strain pt112-dic-11 (MN729613.1); nedicistrovirus (NediV, JQ898341.1); Sanxia picorna-like virus 12 (KX883723.1); Picornavirales sp. isolates s64-k141_2464283 (MZ678982.1) and R35-k141_316374 (MZ678988.1); and a *Pallasea cancelloides* TSA sequence (GEQX01016691.1).

### Identification of candidate IGR IRESs

IGRs were identified using BLASTN (http://www.ncbi.nlm.nih.gov/BLAST) searches of nucleotide collection (nr/nt) and TSA sequences, and BLASTX searches of nonredundant protein (nr) and TSA protein (tsa_nr) sequences in the NCBI database. Nucleotide searches used the parameters: E, 1000; word size, 11; match/mismatch scores, 1/1; gap costs, 2/1. Polypeptide searches used the parameters: E, 1000; word size, 6; Matrix: BLOSUM62; gap costs, 9/1. Hits were characterized by 6-frame translation to identify viral fragments. Amino acid sequences were analyzed to verify that the ORF1 carboxy-terminal region encoded the 3D polymerase and that ORF2 encoded P1 capsid proteins. ORF2 sequences were aligned against dicistrovirus sequences using Clustal Omega (http://www.ebi.ac.uk/Tools/msa/clustalo) to identify potential initiation codons and the approximate 3′ border of potential IRESs. IGR sequences were aligned using EMBOSS Matcher (http://www.ebi.ac.uk/Tools/psa/emboss_matcher/nucleotide.html) and Clustal Omega. 3CD and P1 sequences were aligned using Clustal Omega (default parameters).

### Modeling of IGR IRES structures

Secondary structures were identified using Mfold (Zuker 2003) and tertiary structures were modeled using pKiss (http://bibiserv2.cebitec.uni-bielefeld.de/pkiss) (Janssen and Giegerich 2015) using default parameters. Structural models were refined by comparison with related sequences and on the basis of data from mutational analyses.

### Plasmids

Transcription vectors for $tRNA^{Ser}$ and $tRNA_i^{Met}$ and expression vectors for $His_6$-tagged eIF1, eIF1A, eIF4A, eIF4B, $eIF4G_{736–1115}$, *Escherichia coli* methionyl tRNA synthetase (MetRS), SERBP1, eRF1, and a truncated form of eRF3 lacking a.a. 1–138 have been described (Pestova et al. 1996, 1998; Lomakin et al. 2000, 2006; Heaton et al. 2001; Pestova and Hellen 2001; Alkalaeva et al. 2006; Pisarev et al. 2007; Skabkin et al. 2013; Zinoviev et al. 2015). Transcription vectors for IGR-containing mRNAs (GeneWiz) contain a stable hairpin (5′-GGCTCGAGGCCCGGTGACGGGCC TCGGGCC-3′ [ΔG = −32.70 kcal/mol]) and the viral sequence, downstream from a T7 promoter. pUC57-NediV (wt) contained these elements and NediV nt 1161–1606, inserted between BamH1 and XbaI sites of pUC57, and was used to generate mutated variants. pUC57-NediV(wt) contained these elements and NediV nt 1161–1606, inserted between BamH1 and XbaI sites of pUC57, and was used to generate mutated variants. pUC57-APLV1(wt) contained a T7 promoter, the nucleotides that form the stable hairpin and APLV1 nt 5337–5772, inserted between BamH1 and EcoRV sites of pUC57. Start-to-stop (GCU-UAA) and seryl variants (GCU-UCU) contained GCU start codon to UAA stop codon or to UCU (Serine) codon substitutions, respectively. The $APLV1_{[GCU-UCU]}$ variant was used to generate additional mutants. The vectors for truncated NediV and APLV1 IGR IRES variants contained a T7 promoter followed by NediV nt 1327–1606, 1343–1606 or 1351–1606, APLV1 nt 5434–5772 or 5459–5772, and EcoRV and EcoRI restriction sites.

The plasmids for NediV reading frame selection were prepared using IRES variants with the UCU (Ser) codon placed in +1, +2, or +3 reading frames by inserting G, GC, and GCT nucleotides, respectively, immediately upstream of the TCT triplet.

Transcription vectors for hybrid NediV–APLV1 and NediV–CrPV IGR mRNAs contained a T7 promoter and NediV nt 1327–1455 + APLV1 nt 5565–5606 (NediV[d1/d2] + APLV1[d3]), or NediV nt 1327–1455 + CrPV nt 6174–6320 (NediV[d1/d2] + CrPV[d3]). The NediV[d1/d3] + CrPV[d2] vector contained CrPV nt 6096–6132 instead of NediV nt 1399–1442.

$pUC57\text{-}APLV1_{\Delta 5523–53+AU}$ and $pUC57\text{-}APLV1_{\Delta 5523–53+AUAU}$ were made by replacing APLV1 nt 5523–5553 in pUC57-APLV1 (wt) by the sequences AT and ATAT, respectively. pUC57-CrPV (wt) contains a BamHI site, a T7 promoter, CrPV nt 5997–6320 and EcoRV and EcoRI restriction sites. The pUC57-HalV(wt) vector contained a T7 promoter followed by HalV nt 6268–6483 and EcoRV and EcoRI restriction sites (Abaeva et al. 2020).

pUC57-5′Stem-NediV (nt 1161–2389) was made (GeneWiz) by inserting DNA corresponding to a T7 promoter, the stable hairpin and NediV nt 1161–2389 between BamH1 and EcoRV sites of pUC57. The transcribed mRNA encodes a 299 a.a.-long (32.2 kDa) NediV ORF2 fragment, with 8 in-frame AUG substitutions to increase [$^{35}$S]-methionine incorporation during translation. pUC57-NediV + 5 kDa contained these elements, NediV nt 1161–2540 and a sequence encoding a $His_6$ tag. The transcribed mRNA encodes a 345 a.a.-long (37.4 kDa) NediV ORF2 fragment,

with 9 in-frame AUG substitutions to increase [$^{35}$S]-methionine incorporation during translation. The CrPV dual luciferase vector has been described (Wilson et al. 2000b). All tRNAs and mRNAs were transcribed in vitro using T7 polymerase.

## Purification of factors, ribosomal subunits, and aminoacylation of tRNA

Native eIF2, eIF3, eEF1H, eEF2, total aa-tRNA synthetases and 40S and 60S ribosomal subunits were purified from rabbit reticulocyte lysate (Green Hectares) (Pisarev et al. 2007; Zinoviev et al. 2020). Recombinant eIF1, eIF1A, eIF4A, eIF4B and eIF4G$_{736–1115}$, eRF1, eRF3, *E. coli* methionyl tRNA synthetase, and SERBP1 were purified after expression in *E. coli* (Heaton et al. 2001; Alkalaeva et al. 2006; Lomakin et al. 2006; Pisarev et al. 2007; Zinoviev et al. 2020). Insect 40S and 60S subunits were purified from *S. frugiperda* cell-free extract (Promega) (Abaeva et al. 2020). Native ribosomes were purified from 400 µL RRL (Promega), which was layered onto 10%–30% sucrose density gradients in buffer A (2 mM DTT, 100 mM potassium acetate, 20 mM Tris [pH 7.5], 2.5 mM magnesium chloride, 1 mM ATP, 0.4 mM GTP, and 0.25 mM spermidine) and centrifuged at 53,000 rpm for 90 min at 4°C. Fractions were collected and ribosomes were monitored by absorbance at 260 nm. The bacterial toxin RelE was a gift from V. Ramakrishnan (Neubauer et al. 2009).

Native total calf liver tRNA (Promega) and in vitro transcribed tRNA$^{Ser}$ were aminoacylated using native aminoacyl-tRNA synthetases. tRNA$_i^{Met}$ was aminoacylated with recombinant MetRS and [$^{35}$S]-methionine (>37.0 TBq/mmol; PerkinElmer) (Pisarev et al. 2007; Zinoviev et al. 2020).

## Assembly and analysis of ribosomal complexes

For toeprinting analysis, ribosomal complexes were assembled by incubating 1 pmol mRNA for 5 min at 37°C in a 40 µL reaction volume containing buffer A, 3 pmol 40S subunits, 4.5 pmol 60S subunits or both, and 30 pmol eRF1/eRF3, 6 pmol eEF2 and 18 pmol SERBP1, as indicated. The elongation competence of 80S complexes was assayed by supplementing reaction mixtures with combinations of 6 pmol eEF2, 6 pmol eEF1H, 500 µg/mL cycloheximide, aminoacylated native unfractionated total tRNA (Σaa-tRNA) or in vitro transcribed Ser-tRNA$^{Ser}$ (3 pmol each). Incubation continued for 10 min at 37°C. Primer extension analysis of the assembled complexes was done (Pisarev et al. 2007) using avian myeloblastosis virus reverse transcriptase (AMV RT) (Promega) and $^{32}$P-labeled primer complementary to NediV nt 1566–87, APLV1 nt 5729–50, HalV nt 6458–72 or CrPV nt 6304–19, as appropriate. cDNA products were resolved in 6% polyacrylamide sequencing gels followed by autoradiography.

## Analysis of ribosomal complexes by sucrose density gradient centrifugation

Ribosomal complexes were formed by incubating 10 pmol [α-$^{32}$P]-labeled NediV IGR IRES mRNA with 30 pmol 40S subunits and 40 pmol 60S subunits in buffer A for 15 min at 37°C, and then resolved by centrifugation through 10%–30% sucrose density gradients in buffer A in a Beckman SW55 rotor at 53,000 rpm for 90 min at 4°C. The optical density of fractionated gradients was measured at 260 nm, and the presence of [$^{32}$P]-labeled mRNA was monitored by Cherenkov counting.

## RelE cleavage

Analysis of ribosome-bound mRNA cleavage by RelE in the presence or absence of eEF2 was done as described (Skabkin et al. 2013; Abaeva et al. 2020). An amount of 3 pmol ribosomal complexes was incubated with 40 pmol RelE for 10 min at 37°C. mRNA was then phenol-extracted and analyzed by primer extension.

## Translation in RRL

mRNAs were translated using the Flexi RRL system (Promega) (25 µL reaction volume). An amount of 10 pmol mRNA was preincubated in buffer A with 15 pmol 40S subunits with or without 15 pmol 60S subunits at 37°C for 15 min, supplemented with RRL and [$^{35}$S]-methionine and incubated for 90 min at 30°C. Translation products were analyzed by electrophoresis using NuPAGE 4%–12% Bis-Tris precast gels (Invitrogen), followed by autoradiography.

## Quantification

All in vitro experiments were repeated at least three times. Representative gel images are shown. Gel quantification was done by overnight phosphoimaging with a BAS-IP SR 2040 E Super Resolution Storage phosphor screen followed by imaging using an Amersham Typhoon IP biomolecular imager (GE Healthcare). Toeprints were quantified as a percentage of total radiolabeled cDNA using ImageQuant TL v8.2.

## ACKNOWLEDGMENTS

This research was funded by the National Institutes of Health (R01 AI123406 and R01 GM097014 to C.U.T.H. R35 GM122602 to T.V.P.). We thank V. Ramakrishnan for the gift of RelE.

*Received January 17, 2023; accepted March 27, 2023.*

## REFERENCES

Abaeva IS, Vicens Q, Bochler A, Soufari H, Simonetti A, Pestova TV, Hashem Y, Hellen CU. 2020. The Halastavi árva virus intergenic region IRES promotes translation by the simplest possible initiation mechanism. *Cell Rep* **33:** 108476. doi:10.1016/j.celrep.2020.108476

Alkalaeva EZ, Pisarev AV, Frolova LY, Kisselev LL, Pestova TV. 2006. *In vitro* reconstitution of eukaryotic translation reveals cooperativity between release factors eRF1 and eRF3. *Cell* **125:** 1125–1136. doi:10.1016/j.cell.2006.04.035

Andreev D, Hauryliuk V, Terenin I, Dmitriev S, Ehrenberg M, Shatsky I. 2008. The bacterial toxin RelE induces specific mRNA cleavage in the A site of the eukaryote ribosome. *RNA* **14:** 233–239. doi:10.1261/rna.693208

Arhab Y, Bulakhov AG, Pestova TV, Hellen CUT. 2020. Dissemination of internal ribosomal entry sites (IRES) between viruses by horizontal gene transfer. *Viruses* **12:** 612. doi:10.3390/v12060612

Arhab Y, Miścicka A, Pestova TV, Hellen CUT. 2022. Horizontal gene transfer as a mechanism for the promiscuous acquisition of distinct classes of IRES by avian caliciviruses. *Nucleic Acids Res* **50:** 1052–1068. doi:10.1093/nar/gkab1243

Babendure JR, Babendure JL, Ding JH, Tsien RY. 2006. Control of mammalian translation by mRNA structure near caps. *RNA* **12:** 851–861. doi:10.1261/rna.2309906

Brown A, Baird MR, Yip MC, Murray J, Shao S. 2018. Structures of translationally inactive mammalian ribosomes. *Elife* **7:** e40486. doi:10.7554/eLife.40486

Chen YM, Sadiq S, Tian JH, Chen X, Lin XD, Shen JJ, Chen H, Hao ZY, Wille M, Zhou ZC, et al. 2022. RNA viromes from terrestrial sites across China expand environmental viral diversity. *Nat Microbiol* **7:** 1312–1323. doi:10.1038/s41564-022-01180-2

Costantino D, Kieft JS. 2005. A preformed compact ribosome-binding domain in the cricket paralysis-like virus IRES RNAs. *RNA* **11:** 332–343. doi:10.1261/rna.7184705

Costantino DA, Pfingsten JS, Rambo RP, Kieft JS. 2008. tRNA-mRNA mimicry drives translation initiation from a viral IRES. *Nat Struct Mol Biol* **15:** 57–64. doi:10.1038/nsmb1351

Edgar RC, Taylor J, Lin V, Altman T, Barbera P, Meleshko D, Lohr D, Novakovsky G, Buchfink B, Al-Shayeb B, et al. 2022. Petabase-scale sequence alignment catalyses viral discovery. *Nature* **602:** 142–147. doi:10.1038/s41586-021-04332-2

Fernández IS, Bai XC, Murshudov G, Scheres SH, Ramakrishnan V. 2014. Initiation of translation by cricket paralysis virus IRES requires its translocation in the ribosome. *Cell* **157:** 823–831. doi:10.1016/j.cell.2014.04.015

Flis J, Holm M, Rundlet EJ, Loerke J, Hilal T, Dabrowski M, Bürger J, Mielke T, Blanchard SC, Spahn CMT, et al. 2018. tRNA Translocation by the eukaryotic 80S ribosome and the impact of GTP hydrolysis. *Cell Rep* **25:** 2676–2688.e7. doi:10.1016/j.celrep.2018.11.040

Hatakeyama Y, Shibuya N, Nishiyama T, Nakashima N. 2004. Structural variant of the intergenic internal ribosome entry site elements in dicistroviruses and computational search for their counterparts. *RNA* **10:** 779–786. doi:10.1261/rna.5208104

Heaton JH, Dlakic WM, Dlakic M, Gelehrter TD. 2001. Identification and cDNA cloning of a novel RNA-binding protein that interacts with the cyclic nucleotide-responsive sequence in the type-1 plasminogen activator inhibitor mRNA. *J Biol Chem* **276:** 3341–3347. doi:10.1074/jbc.M006538200

Jackson RJ, Hellen CU, Pestova TV. 2010. The mechanism of eukaryotic translation initiation and principles of its regulation. *Nat Rev Mol Cell Biol* **11:** 113–127. doi:10.1038/nrm2838

Jan E, Sarnow P. 2002. Factorless ribosome assembly on the internal ribosome entry site of cricket paralysis virus. *J Mol Biol* **324:** 889–902. doi:10.1016/s0022-2836(02)01099-9

Jan E, Kinzy TG, Sarnow P. 2003. Divergent tRNA-like element supports initiation, elongation, and termination of protein biosynthesis. *Proc Natl Acad Sci* **100:** 15410–15415. doi:10.1073/pnas.2535183100

Jang CJ, Jan E. 2010. Modular domains of the *Dicistroviridae* intergenic internal ribosome entry site. *RNA* **16:** 1182–1195. doi:10.1261/rna.2044610

Janssen S, Giegerich R. 2015. The RNA shapes studio. *Bioinformatics* **31:** 423–425. doi:10.1093/bioinformatics/btu649

Kerr CH, Ma ZW, Jang CJ, Thompson SR, Jan E. 2016. Molecular analysis of the factorless internal ribosome entry site in *Cricket Paralysis virus* infection. *Sci Rep* **6:** 37319. doi:10.1038/srep37319

Kerr CH, Wang QS, Moon KM, Keatings K, Allan DW, Foster LJ, Jan E. 2018. IRES-dependent ribosome repositioning directs translation of a +1 overlapping ORF that enhances viral infection. *Nucleic Acids Res* **46:** 11952–11967. doi:10.1093/nar/gky1121

Kieft JS. 2008. Viral IRES RNA structures and ribosome interactions. *Trends Biochem Sci* **33:** 274–283. doi:10.1016/j.tibs.2008.04.007

Koh CS, Brilot AF, Grigorieff N, Korostelev AA. 2014. Taura syndrome virus IRES initiates translation by binding its tRNA-mRNA-like structural element in the ribosomal decoding center. *Proc Natl Acad Sci* **111:** 9139–9144. doi:10.1073/pnas.1406335111

Lomakin IB, Hellen CU, Pestova TV. 2000. Physical association of eukaryotic initiation factor 4G (eIF4G) with eIF4A strongly enhances binding of eIF4G to the internal ribosomal entry site of encephalomyocarditis virus and is required for internal initiation of translation. *Mol Cell Biol* **20:** 6019–6029. doi:10.1128/MCB.20.16.6019-6029.2000

Lomakin IB, Shirokikh NE, Yusupov MM, Hellen CU, Pestova TV. 2006. The fidelity of translation initiation: reciprocal activities of eIF1, IF3 and YciH. *EMBO J* **25:** 196–210. doi:10.1038/sj.emboj.7600904

López-Bueno A, Rastrojo A, Peiró R, Arenas M, Alcamí A. 2015. Ecological connectivity shapes quasispecies structure of RNA viruses in an antarctic lake. *Mol Ecol* **24:** 4812–4825. doi:10.1111/mec.13321

Mailliot J, Martin F. 2018. Viral internal ribosomal entry sites: four classes for one goal. *Wiley Interdiscip Rev RNA* **9**. doi:10.1002/wrna.1458

Martinez-Salas E, Francisco-Velilla R, Fernandez-Chamorro J, Embarek AM. 2018. Insights into structural and mechanistic features of viral IRES elements. *Front Microbiol* **8:** 2629. doi:10.3389/fmicb.2017.02629

Muhs M, Hilal T, Mielke T, Sanbonmatsu KY, Pestova TV, Spahn CM. 2015. Cryo-EM of ribosomal 80S complexes with termination factors reveals the translocated cricket paralysis virus IRES. *Mol Cell* **57:** 422–432. doi:10.1016/j.molcel.2014.12.016

Muhs M, Yamamoto H, Ismer J, Takaku H, Nashimoto M, Uchiumi T, Nakashima N, Mielke T, Hildebrand PW, Nierhaus KH, et al. 2011. Structural basis for the binding of IRES RNAs to the head of the ribosomal 40S subunit. *Nucleic Acids Res* **39:** 5264–5275. doi:10.1093/nar/gkr114

Nakashima N, Uchiumi T. 2009. Functional analysis of structural motifs in dicistroviruses. *Virus Res* **139:** 137–147. doi:10.1016/j.virusres.2008.06.006

Naumenko SA, Logacheva MD, Popova NV, Klepikova AV, Penin AA, Bazykin GA, Etingova AE, Mugue NS, Kondrashov AS, Yampolsky LY. 2017. Transcriptome-based phylogeny of endemic Lake Baikal amphipod species flock: fast speciation accompanied by frequent episodes of positive selection. *Mol Ecol* **26:** 536–553. doi:10.1111/mec.13927

Neubauer C, Gao YG, Andersen KR, Dunham CM, Kelley AC, Hentschel J, Gerdes K, Ramakrishnan V, Brodersen DE. 2009. The structural basis for mRNA recognition and cleavage by the ribosome-dependent endonuclease RelE. *Cell* **139:** 1084–1095. doi:10.1016/j.cell.2009.11.015

Ng TF, Marine R, Wang C, Simmonds P, Kapusinszky B, Bodhidatta L, Oderinde BS, Wommack KE, Delwart E. 2012. High variety of known and new RNA and DNA viruses of diverse origins in untreated sewage. *J Virol* **86:** 12161–12175. doi:10.1128/JVI.00869-12

Nishiyama T, Yamamoto H, Shibuya N, Hatakeyama Y, Hachimori A, Uchiumi T, Nakashima N. 2003. Structural elements in the internal ribosome entry site of *Plautia stali* intestine virus responsible for binding with ribosomes. *Nucleic Acids Res* **31:** 2434–2442. doi:10.1093/nar/gkg336

Nishiyama T, Yamamoto H, Uchiumi T, Nakashima N. 2007. Eukaryotic ribosomal protein RPS25 interacts with the conserved loop region in a dicistroviral intergenic internal ribosome entry site. *Nucleic Acids Res* **35:** 1514–1521. doi:10.1093/nar/gkl1121

Pestova TV, Hellen CU. 2001. Preparation and activity of synthetic unmodified mammalian $tRNA_i^{Met}$ in initiation of translation *in vitro*. *RNA* **7:** 1496–1505. doi:10.1017/s135583820101038x

Pestova TV, Hellen CU. 2003. Translation elongation after assembly of ribosomes on the Cricket paralysis virus internal ribosomal entry site without initiation factors or initiator tRNA. *Genes Dev* **17:** 181–186. doi:10.1101/gad.1040803

Pestova TV, Hellen CU, Shatsky IN. 1996. Canonical eukaryotic initiation factors determine initiation of translation by internal ribosomal entry. *Mol Cell Biol* **16:** 6859–6869. doi:10.1128/MCB.16.12.6859

Pestova TV, Borukhov SI, Hellen CU. 1998. Eukaryotic ribosomes require initiation factors 1 and 1A to locate initiation codons. *Nature* **394:** 854–859. doi:10.1038/29703

Pestova TV, Lomakin IB, Hellen CU. 2004. Position of the CrPV IRES on the 40S subunit and factor dependence of IRES/80S ribosome assembly. *EMBO Rep* **5:** 906–913. doi:10.1038/sj.embor.7400240

Petrov A, Grosely R, Chen J, O'Leary SE, Puglisi JD. 2016. Multiple parallel pathways of translation initiation on the CrPV IRES. *Mol Cell* **62:** 92–103. doi:10.1016/j.molcel.2016.03.020

Pfingsten JS, Costantino DA, Kieft JS. 2006. Structural basis for ribosome recruitment and manipulation by a viral IRES RNA. *Science* **314:** 1450–1454. doi:10.1126/science.1133281

Pfingsten JS, Castile AE, Kieft JS. 2010. Mechanistic role of structurally dynamic regions in *Dicistroviridae* IGR IRESs. *J Mol Biol* **395:** 205–217. doi:10.1016/j.jmb.2009.10.047

Pisarev AV, Unbehaun A, Hellen CU, Pestova TV. 2007. Assembly and analysis of eukaryotic translation initiation complexes. *Methods Enzymol* **430:** 147–177. doi:10.1016/S0076-6879(07)30007-4

Pisareva VP, Pisarev AV, Fernández IS. 2018. Dual tRNA mimicry in the Cricket Paralysis Virus IRES uncovers an unexpected similarity with the Hepatitis C Virus IRES. *Elife* **7:** e34062. doi:10.7554/eLife.34062

Ren Q, Wang QS, Firth AE, Chan MM, Gouw JW, Guarna MM, Foster LJ, Atkins JF, Jan E. 2012. Alternative reading frame selection mediated by a tRNA-like domain of an internal ribosome entry site. *Proc Natl Acad Sci* **109:** E630–E639. doi:10.1073/pnas.1111303109

Ruehle MD, Zhang H, Sheridan RM, Mitra S, Chen Y, Gonzalez RL, Cooperman BS, Kieft JS. 2015. A dynamic RNA loop in an IRES affects multiple steps of elongation factor-mediated translation initiation. *Elife* **4:** e08146. doi:10.7554/eLife.08146

Sasaki J, Nakashima N. 1999. Translation initiation at the CUU codon is mediated by the internal ribosome entry site of an insect picorna-like virus in vitro. *J Virol* **73:** 1219–1226. doi:10.1128/JVI.73.2.1219-1226.1999

Sasaki J, Nakashima N. 2000. Methionine-independent initiation of translation in the capsid protein of an insect RNA virus. *Proc Natl Acad Sci* **97:** 1512–1515. doi:10.1073/pnas.010426997

Schüler M, Connell SR, Lescoute A, Giesebrecht J, Dabrowski M, Schroeer B, Mielke T, Penczek PA, Westhof E, Spahn CM. 2006. Structure of the ribosome-bound cricket paralysis virus IRES RNA. *Nat Struct Mol Biol* **13:** 1092–1096. doi:10.1038/nsmb1177

Shetty S, Hofstetter J, Battaglioni S, Ritz D, Hall MN. 2023. TORC1 phosphorylates and inhibits the ribosome preservation factor Stm1 to activate dormant ribosomes. *EMB0O J* **42:** e112344. doi:10.15252/embj.2022112344

Shi M, Lin XD, Tian JH, Chen LJ, Chen X, Li CX, Qin XC, Li J, Cao JP, Eden JS, et al. 2016. Redefining the invertebrate RNA virosphere. *Nature* **540:** 539–543. doi:10.1038/nature20167

Skabkin MA, Skabkina OV, Hellen CU, Pestova TV. 2013. Reinitiation and other unconventional posttermination events during eukaryotic translation. *Mol Cell* **51:** 249–264. doi:10.1016/j.molcel.2013.05.026

Smith PR, Loerch S, Kunder N, Stanowick AD, Lou TF, Campbell ZT. 2021. Functionally distinct roles for eEF2K in the control of ribosome availability and p-body abundance. *Nat Commun* **12:** 6789. doi:10.1038/s41467-021-27160-4

Šponer J, Bussi G, Krepl M, Banáš P, Bottaro S, Cunha RA, Gil-Ley A, Pinamonti G, Poblete S, Jurečka P, et al. 2018. RNA structural dynamics as captured by molecular simulations: a comprehensive overview. *Chem Rev* **118:** 4177–4338. doi:10.1021/acs.chemrev.7b00427

Susorov D, Zakharov N, Shuvalova E, Ivanov A, Egorova T, Shuvalov A, Shatsky IN, Alkalaeva E. 2018. Eukaryotic translation elongation factor 2 (eEF2) catalyzes reverse translocation of the eukaryotic ribosome. *J Biol Chem* **293:** 5220–5229. doi:10.1074/jbc.RA117.000761

Thompson SR, Gulyas KD, Sarnow P. 2001. Internal initiation in *Saccharomyces cerevisiae* mediated by an initiator tRNA/eIF2-independent internal ribosome entry site element. *Proc Natl Acad Sci* **98:** 12972–12977. doi:10.1073/pnas.241286698

Waldron FM, Stone GN, Obbard DJ. 2018. Metagenomic sequencing suggests a diversity of RNA interference-like responses to viruses across multicellular eukaryotes. *PLoS Genet* **14:** e1007533. doi:10.1371/journal.pgen.1007533

Wilson JE, Pestova TV, Hellen CU, Sarnow P. 2000a. Initiation of protein synthesis from the A site of the ribosome. *Cell* **102:** 511–520. doi:10.1016/s0092-8674(00)00055-6

Wilson JE, Powell MJ, Hoover SE, Sarnow P. 2000b. Naturally occurring dicistronic cricket paralysis virus RNA is regulated by two internal ribosome entry sites. *Mol Cell Biol* **20:** 4990–4999. doi:10.1128/MCB.20.14.4990-4999.2000

Wolf YI, Silas S, Wang Y, Wu S, Bocek M, Kazlauskas D, Krupovic M, Fire A, Dolja VV, Koonin EV. 2020. Doubling of the known set of RNA viruses by metagenomic analysis of an aquatic virome. *Nat Microbiol* **5:** 1262–1270. doi:10.1038/s41564-020-0755-4

Yamamoto H, Nakashima N, Ikeda Y, Uchiumi T. 2007. Binding mode of the first aminoacyl-tRNA in translation initiation mediated by *Plautia stali* intestine virus internal ribosome entry site. *J Biol Chem* **282:** 7770–7776. doi:10.1074/jbc.M610887200

Yang S, Mao Q, Wang Y, He J, Yang J, Chen X, Xiao Y, He Y, Zhao M, Lu J, et al. 2022. Expanding known viral diversity in plants: virome of 161 species alongside an ancient canal. *Environ Microbiome* **17:** 58. doi:10.1186/s40793-022-00453-x

Yesselman JD, Denny SK, Bisaria N, Herschlag D, Greenleaf WJ, Das R. 2019. Sequence-dependent RNA helix conformational preferences predictably impact tertiary structure formation. *Proc Natl Acad Sci* **116:** 16847–16855. doi:10.1073/pnas.1901530116

Zell R, Groth M, Selinka L, Selinka HC. 2022. Picorna-like viruses of the Havel river, Germany. *Front Microbiol* **13:** 865287. doi:10.3389/fmicb.2022.865287

Zhu J, Korostelev A, Costantino DA, Donohue JP, Noller HF, Kieft JS. 2011. Crystal structures of complexes containing domains from two viral internal ribosome entry site (IRES) RNAs bound to the 70S ribosome. *Proc Natl Acad Sci* **108:** 1839–1844. doi:10.1073/pnas.1018582108

Zinoviev A, Hellen CUT, Pestova TV. 2015. Multiple mechanisms of reinitiation on bicistronic calicivirus mRNAs. *Mol Cell* **57:** 1059–1073. doi:10.1016/j.molcel.2015.01.039

Zinoviev A, Goyal A, Jindal S, LaCava J, Komar AA, Rodnina MV, Hellen CUT, Pestova TV. 2018. Functions of unconventional mammalian translational GTPases GTPBP1 and GTPBP2. *Genes Dev* **32:** 1226–1241. doi:10.1101/gad.314724.118

Zinoviev A, Hellen CUT, Pestova TV. 2020. *In vitro* characterization of the activity of the mammalian RNA exosome on mRNAs in ribosomal translation complexes. *Meth Mol Biol* **2062:** 327–354. doi:10.1007/978-1-4939-9822-7_16

Zuker M. 2003. Mfold web server for nucleic acid folding and hybridization prediction. *Nucleic Acids Res* **31:** 3406–3415. doi:10.1093/nar/gkg595

*See the following page for* ***Meet the First Authors***

## MEET THE FIRST AUTHORS

Anna Miścicka

Kristen Lu

***Meet the First Author(s)* is an editorial feature within RNA, in which the first author(s) of research-based papers in each issue have the opportunity to introduce themselves and their work to readers of RNA and the RNA research community. Anna Miścicka and Kristen Lu are joint first authors of this paper, "Initiation of translation on nedicistrovirus and related intergenic region IRESs by their factor-independent binding to the P site of 80S ribosomes." Anna obtained her PhD degree in Warsaw, Poland, and started her postdoctoral fellowship in the Hellen/Pestova laboratory. Kristen was previously a graduate student in the Hellen/Pestova laboratory and the work published in this paper reflects her dissertation project. She is now the Global Alzheimer's Forecasting Lead at Biogen Inc., a biotech company based in Cambridge, Massachusetts.**

**What are the major results described in your paper and how do they impact this branch of the field?**

Our paper describes a novel subclass of intergenic region IRESs that use factor-independent mechanisms to bind to the P site of 80S ribosomes. This work continues to support the ever-increasing breadth of IRES biology and how either conservation or loss of structural elements has significant mechanistic consequences for protein translation.

**What led you to study RNA or this aspect of RNA science?**

**AM:** I was always interested in protein synthesis. During my PhD studies, I was working on non-AUG initiation in yeast; thus IGR IRES-mediated initiation, which also involves non-AUG initiation, was very exciting for me.

**KL:** I have always been interested in viruses and how they have evolved various methods of coopting host machinery for biological processes like translation. Single-stranded RNA viruses, in particular, are a marvelous example of how a small piece of genetic information leads to complex behaviors, more fitting for a higher-order organism but somehow contained within a compact structure.

**During the course of these experiments, were there any surprising results or particular difficulties that altered your thinking and subsequent focus?**

The NediV-like IGR IRESs have some unique features vs. the previously identified IGR IRESs. For example, the small UACUA motif in domain 2 appears to be very crucial as small mutations in this region can result in impairment of ribosomal complex formation, but there is still work to be done to understand how this motif interacts with the ribosome.

**What are some of the landmark moments that provoked your interest in science or your development as a scientist?**

**AM:** Since I was a child, I was always very curious how the world around me works and I love to learn new things. Being a scientist feeds my curiosity for discovery and brings me joy of constant learning.

**KL:** I have always appreciated the ways in which scientific discovery and research consistently honor empiricism—specifically, I was enamored with the objective interpretation of experimental results paired with a dynamic willingness to revise hypotheses. Though I am no longer in the research field, I continue to value the importance of anchoring to facts, developing theories, and being flexible when facts do not align to theories.

**What are your subsequent near- or long-term career plans?**

**AM:** I hope to further keep my curiosity for science, develop as a researcher and one day become a PI.

**KL:** I would like to continue my development and training in my current role; in the future, my goal is to transition to leading commercialization of a drug or therapeutic franchise.

**What were the strongest aspects of your collaboration as co-first authors?**

**AM:** For me, it was the possibility of sharing experiences and points of view on experimental approaches and results from those experiments. Collaboration allows us to see the research with a wider perspective.

**KL:** The organization and continuity of experimental designs and results were so critical to advancing this collaboration. There were many mutants created for the experiments shown in the paper, complex experimental designs that would need to be repeated to ensure reproducibility of results, and a shared perspective on how to approach the analysis.